

Multiscale Comparative Connectomics

Vivek Gopalakrishnan^{1,*}, Jaewon Chung¹, Eric Bridgeford², Benjamin D. Pedigo¹, Jesús Arroyo³, Lucy Upchurch⁴, G. Allan Johnson^{4,5}, Nian Wang⁶, Youngser Park⁷, Carey E. Priebe^{7,8}, and Joshua T. Vogelstein^{1,7}

Abstract. A connectome is a map of the structural and/or functional connections in the brain. This information-rich representation has the potential to transform our understanding of the relationship between patterns in brain connectivity and neurological processes, disorders, and diseases. However, existing computational techniques used to analyze connectomes are often insufficient for interrogating multi-subject connectomics datasets: we illustrate numerous conceptual and practical deficiencies with widely-used connectomics methods including weak (and often invalid) theoretical foundations, meager statistical power in simulation settings, and an inability to recover known neurobiological information from the simplest connectomics datasets. To enable more rigorous comparative connectomics analysis, we introduce robust and interpretable statistical methods motivated by recent theoretical advances in random graph models. These methods facilitate simultaneous analysis of multiple connectomes across different scales of network topology, facilitating the discovery of hierarchical brain structures that vary in relation with phenotypic profiles. We validated these methods through extensive simulation studies, as well as synthetic and real-data experiments. Using a set of high-resolution connectomes obtained from genetically distinct mouse strains (including the BTBR mouse—a standard model of autism—and three behavioral wild-types), we show that these methods uncover valuable latent information in multi-subject connectomics data and yield novel insights into the connective correlates of neurological phenotypes.

1 Introduction Understanding how patterns in brain connectivity correlate with observable phenotypes is a central pursuit in neuroscience research. Neuroimaging data is crucial for this goal, and previous computational neuroscientific analyses have helped yield insights into the links between brain connectivity and various neurological phenomena such as cognition [1, 2], neurodevelopment [3–5], the heritability of brain structures [6–8], and the pathology of neurological diseases [9–12]. Derived from neuroimaging data, a connectome, or map of the functional and/or structural connections between distinct brain regions, has recently become an invaluable tool for such analyses, enabling researchers to model the brain as a network and understand its organization with graph theoretical methods [13–17]. Successfully associating phenotypic profiles with variation in the connectome will enable the elucidation of identifiable neurological structures that underlie phenotypes, thereby transforming our understanding of the human brain [18]. However, to fully realize the promise of the connectome, novel statistical approaches that are principled, robust, and reproducible are required for the analysis of this nascent and highly-complex data type [19].

From a mathematical perspective, connectomes can be modeled as a network (or graph) of the interactions between brain regions [20]. In this network, vertices represent discrete parcellations of the brain, and edges represent the functional or structural connections between these brain regions [21]. From a graph theory perspective, the connectome can be further described at multiple hierarchical scales of network topology [22]: at the extremes are the *local scale*, characterized by the features of individual edges and vertices in the connectome, and the *global scale*, characterized by global patterns in brain connectivity and often quantified by a variety of graph-level statistics [23]; the intermediate *regional scale* focuses on the interactions between distinct subsets of brain regions (known as communities or blocks), comprising subgraphs of the connectome [24–28]. Simultaneously considering the local, regional, and global scales of network topology provides a multiscale overview of patterns in brain connectivity.

*Corresponding author: vivekg@mit.edu ¹Department of Biomedical Engineering, Johns Hopkins University ²Department of Biostatistics, Johns Hopkins University ³Department of Mathematics, University of Maryland, College Park ⁴Duke Center for In Vivo Microscopy, Department of Radiology, Duke University ⁵Department of Biomedical Engineering, Duke University ⁶Department of Radiology and Imaging Sciences, Indiana University School of Medicine ⁷Center for Imaging Science, Johns Hopkins University ⁸Department of Applied Mathematics and Statistics, Johns Hopkins University

The fundamental goal of comparative connectome analysis is to identify the multiscale patterns in network architecture that differ across phenotypic groups [29]. However, given the inherent structure of connectomes, special care needs to be taken when designing analytical methods: that is, the naive application of classical statistical tests to network-valued data will produce specious results. In this work, we show that many widely-used methods to analyze connectomes have weak (and often invalid) theoretical foundations, thereby yielding poor statistical performance and spurious inferences. For example, many previous works advocate for the use of graph-level statistics (e.g., clustering coefficient, degree coefficient, number of triangles, etc.) to characterize differences in the connectivity patterns of connectomes. However, this approach is particularly problematic: recent studies have shown that no set of graph statistics can comprehensively describe network topology, as networks with wildly different structures can produce identical graph statistics [30, 31]. Therefore, methods that perform subsequent statistical tests on these graph statistics will produce incorrect insights, and neuroscientific interpretations as to the meaning of these test results will be useless.

To overcome these limitations and enable the rigorous interrogation of multi-subject connectomics datasets, we present inferential statistical methods that provide insight across topological scales of the connectome (Figure 1). Predicated on recent theoretical advances in random graph models, our methods identify neurobiological structures within connectome that are connectively different across multiple categorical or dimensional phenotypes, which we term *signal* components. Specifically, these algorithms can be used to discover signal edges, vertices, and communities within populations of connectomes defined on the same vertex set and are appropriate for analyzing connectomes estimated from either structural or functional neuroimaging data. We formulate these methods as k -sample hypothesis tests, enabling comparisons of connectomes from more than two distinct phenotypic groups. Finally, we show how these methods can be aggregated to perform whole-brain comparisons, in total enabling interrogation of the local, regional, and global scales of network topology.

We demonstrate the efficacy and utility of our multiscale connectomics methods by applying them to an open access dataset of ultrahigh-resolution structural mouse connectomes (derived at a spatial resolution 20,000 times greater than typical human connectomes) [32]. Additionally, we establish the superiority of our proposed methods over prevailing connectomics analysis strategies in extensive simulation studies, and show that the neurobiological insights of our measures of connectivity are orthogonal to existing measures through information-theoretic comparisons.

2 Results

2.1 A multi-subject mouse connectome dataset for algorithmic validation We provide illustrative examples of how our multiscale connectomics methods operate on real-world data by applying them to an open access dataset of whole-brain diffusion magnetic resonance imaging-derived connectomes from four mouse lines: BTBR T+ Itpr3tf/J (BTBR), C57BL/6J (B6), CAST/EiJ (CAST), and DBA/2J (DBA2) [32]. The BTBR mouse strain is a well-studied model that exhibits the core behavioral deficits that characterize autism spectrum disorders (ASD) in humans [33–35]. Additionally, the BTBR mouse has significant neuroanatomical abnormalities including the complete absence of the corpus callosum, a band of nerve fibers connecting the left and right hemispheres of the brain [36, 37]. Therefore, we can use this dataset to determine if our methods will successfully recover previously established neurobiological information. The B6, CAST, and DBA2 mice are genetically distinct strains that do not exhibit ASD-like behaviors. They serve as wild type behavioral controls in these experiments.

For each strain, connectomes were generated from eight age-matched mice ($N = 8$ per strain with a sex distribution of four males and four females) using diffusion tensor imaging (DTI) tractography (for more details, see the Methods §4.9). Improved imaging protocols and custom hardware were developed and implemented in this study to solve existing technical issues with DTI, including an inability to resolve crossing and merging fibers (for more details, see §2.2 of [32]). Each connectome was parcellated using a symmetric Waxholm Space [38, 39], yielding a vertex set with a total of 326 regions of interest (ROIs) bilaterally distributed across the left and right hemispheres. Within a given hemisphere, there

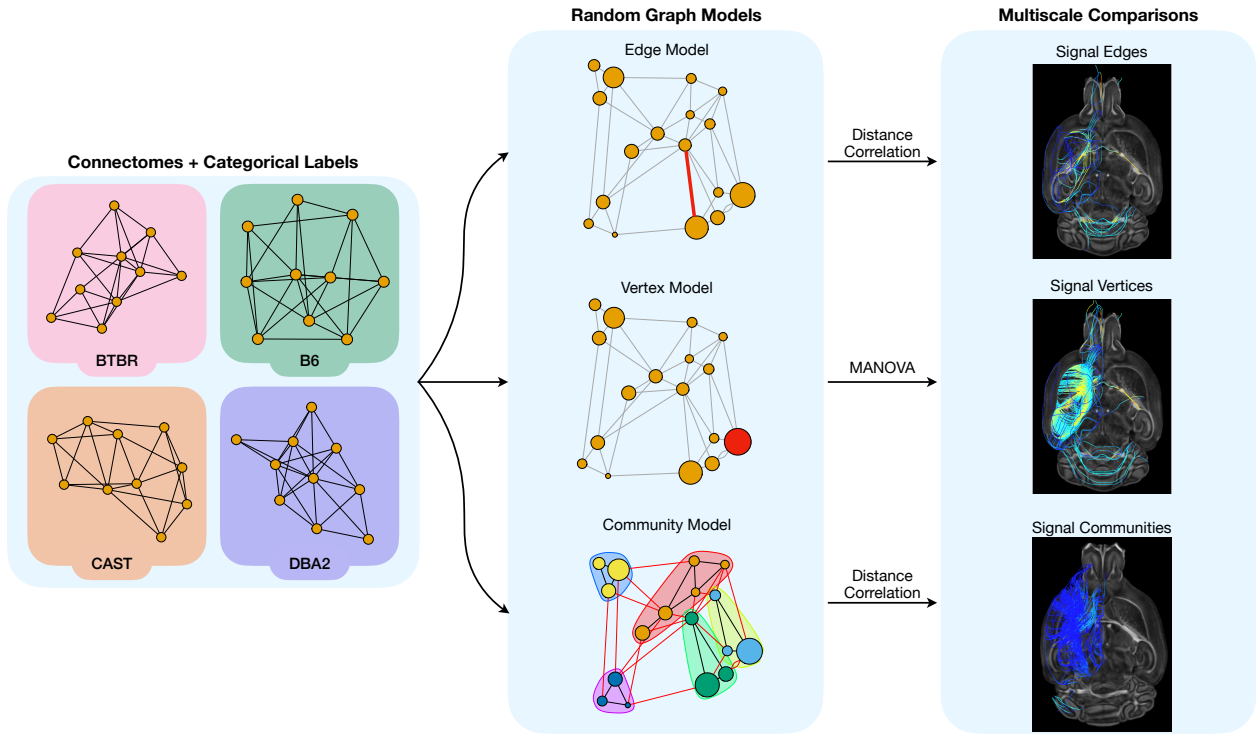


Figure 1: Overview of the statistical framework for multiscale comparative connectomics. (*Left*) All connectomes must be defined on a common set of vertices and have an associated categorical label. Labelled representative networks from four mouse lines whose connectomes we analyze in this work are shown. (*Center*) Connectomes are fit to random graph models that are specifically chosen to model the variation in a network at a given topological scale. (*Right*) Using the categorical labels, k -sample statistical hypothesis tests are applied to the estimated parameters from each model, yielding a set of the signal edges, vertices, and communities across the groups in a given multi-subject connectomics dataset. We visualize identified structures using tractography.

were seven superstructures consisting up multiple ROIs, resulting in a total of 14 distinct communities in each connectome. Heatmaps of the average log-transformed adjacency matrix for each strain with hierarchical community and hemispheric labels are shown in Figure 2.

2.2 Interrogating the *local scale* Illustrative applications of our proposed local scale algorithms, along with comparisons to existing connectomics methods, are provided below. The mathematical formulations of these algorithms for identifying signal edges and signal vertices are provided in the Methods (§4.4).

Identifying signal edges The simplest approach for comparing connectomes is to treat them as a *bag of edges* without considering interactions between the edges [19]. Serially performing univariate statistical tests at each edge enables the discovery of *signal edges* whose neurological connectivity differs across categorical or dimensional phenotypes. This is a well-established analytical approach in connectomics, and many classical statistical tests like one-way analysis of variance (ANOVA) and the Kruskal–Wallis H test are commonly used for edge-wise testing [19, 40, 41]. However, these are tests of equality in *location*: that is, they test whether the mean (or median, in the case of Kruskal–Wallis) weight of a particular edge is statistically different across phenotypes. If the distribution of an edge weight is different across phenotypes but the mean edge weight happens to be equal (for example, if one phenotype is bimodal for a particular weight), ANOVA and Kruskal–Wallis will fail to identify this signal edge. To account for this deficiency, we advocate for the use of Distance Correlation (DCORR)—a previously established universally consistent nonparametric test for equality in distribution [42, 43]—to detect signal edges. DCORR measures the strength of both linear and nonlinear association between

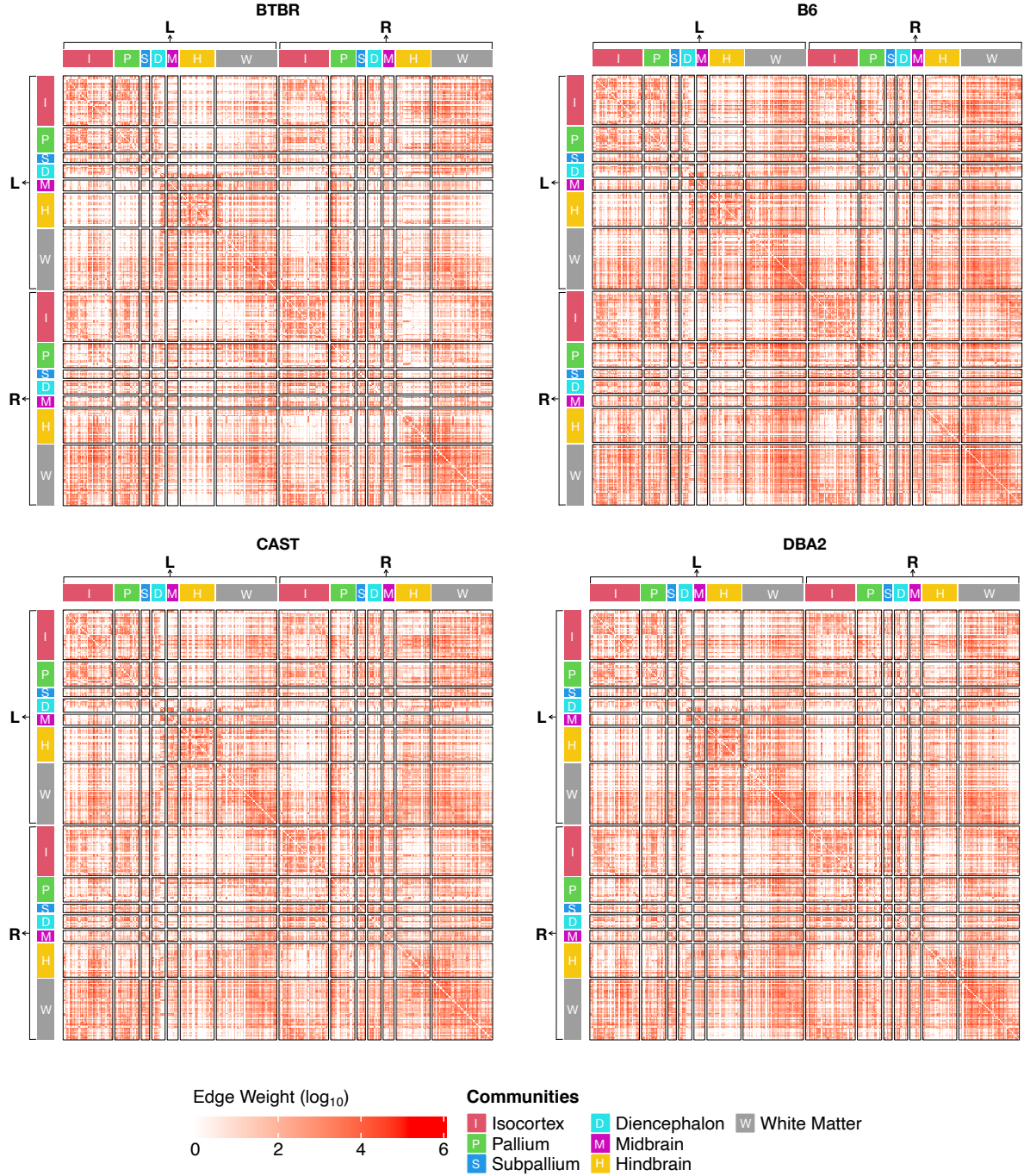


Figure 2: Log-transformed average connectomes for each mouse strain with hierarchical structure labels. Hierarchical labels show the hemispheric and superstructure level. For hemispheric labels, L (R) denotes the left (right) hemisphere. Superstructures are labelled as follows: I) isocortex, P) pallium, S) subpallium, D) diencephalon, M) midbrain, H) hindbrain, and W) white matter. Adapted from [32] with permission.

two random variables (in this case, the edge weight and the phenotypic label), and equals zero if and only if the random variables are independent [42], unlike Pearson's correlation coefficient.

To illustrate the advantages of Dcorr, in the Methods (§4.5), we consider a two-population simulation setting where edge weights are sampled from distinct truncated normal distributions. When all signal edges are different only in their mean, Dcorr, ANOVA, and Kruskal–Wallis all successfully

identify signal edges, and no test outperforms the others in this setting (Supplementary Figure 1A); however, when the mean edge weight is held equal but the variance is different across groups, only Dcorr successfully detects the signal edges (Supplementary Figure 1B). ANOVA and Kruskal–Wallis fail in this scenario because both test for differences in *location* (the mean and median, respectively) across groups, whereas Dcorr tests for differences in *distribution*. This is of particular concern because many popular connectomics methods which aggregate serial edge-wise tests (e.g., the network-based statistic and its various extensions [44–46]) use ANOVA to detect signal edges, and thus their inferences on real-world connectomics data cannot always be trusted.

Using this framework, we identified the signal edges across our four mouse strains. Application of Dcorr showed that no edges were significant at $\alpha = 0.05$ following Holm–Bonferroni correction (for more information on we corrected for multiple comparisons, see the Methods (§4.1)). However, this does not imply that there were no connections between brain regions whose wiring patterns were heterogeneous across different genotypes: because the number of edges we compared across strains was very large (54,946 edges), the strongest signal edge would have had to achieve an uncorrected p -value $< 10^{-6}$ to be deemed statistically significant. Given this well-known limitation imposed by the high-dimensional nature of connectomics data [19], as well as the arbitrary use of $\alpha = 0.05$ as a threshold, we use the ranking of the p -value for each edge to identify the strongest signal edges, not statistical significance.

Note that choosing to rank the p -values or associated test statistics for a set of edges will all produce the same outcome: the edges that are most connectively distinct across different groups will be top ranked in any of these metrics. For example, the edge with the smallest p -value (i.e., strongest signal edge) will also have the largest test statistic. Both of these metrics effectively act as pseudo-dissimilarity measures, quantifying the joint distance between an edge across groups. We choose to report and rank the p -values because we have used rigorous statistical guarantees to formulate our algorithms as inferential hypothesis tests.

A list of the 20 strongest signal edges, along with their corresponding test statistics and p -values, are given in Supplementary Table 1. The strongest signal edge connects the left hemisphere corpus callosum to the right hemisphere striatum. In fact, 13 of the 20 strongest signal edges are adjacent to these two ROIs, demonstrating that the connections emanating from these regions are highly heterogeneous across genotypes. This suggests that instead of looking for signal *edges*, it might be more insightful to interrogate the next hierarchical topological scale of network topology, and look for signal *vertices*.

Identifying signal vertices The ability to discover brain regions that are topologically dissimilar across phenotypes (i.e., *signal vertices*) is critical for scientific and clinical analyses of connectomes, with broad applications such as the establishment of neurological biomarkers and identification of therapeutic targets [47]. Here, we leverage recent advances in the theory of random graph models to propose a principled and robust statistical method for identifying signal vertices. We also demonstrate that this method recovers far more information about ROIs than node-level graph statistics, the predominant method for analyzing vertices in multi-subject connectomics [19, 48, 49].

We use the omnibus embedding (OMNI) [50] — a graph embedding technique — to jointly represent all the connectomes in a multi-subject dataset within a common Euclidean subspace. For each connectome, OMNI jointly maps each vertex to a real-valued vector that corresponds to the vertex’s latent position (see the Methods (§4.3)). This latent position quantifies a given vertex’s probability of connecting to any other vertex in the connectome. Then, for each vertex, we then apply a multivariate statistical test to determine whether the embedding of a specific brain region is different across groups. Previous statistical results have shown that the latent position vectors produced by OMNI are asymptotically Gaussian [51], motivating our use of multivariate analysis of variance (MANOVA) to identify the signal vertices.

To illustrate the advantages of this approach over existing techniques, in the Methods (§4.6), we compare OMNI to two other previously established graph embedding methods: (i) the Exponential ran-

dom graph model (ERGM), which incorporates the exceedingly popular approach of representing each vertex with a vector of node-level graph statistics [52], and (ii) Multivariate Distance Matrix Regression (MDMR) which represents each vertex as a vector of the weights for all adjacent edges [53]. In a two-population simulation setting, we sample graphs from a distribution in which the true number of signal vertices is determined *a priori*. Then, for each vertex, we compute a p -value using each of the three vertex embeddings following Holm–Bonferroni correction. We measure the statistical power of each approach via a Receiver Operating Characteristic (ROC) curve, a performance metric which holistically describes the performance of a binary classifier by characterizing the trade-off between sensitivity and specificity as the discriminant threshold of the classifier (in this case, α) is varied.

Supplementary Figure 2 shows that OMNI is a far superior vertex representation method than the ERGM or MDMR, with an average Area Under the ROC (AUROC) 20% greater than the other two methods. Even in the most challenging simulation settings where the true number of signal vertices is very small, OMNI correctly identifies the vertices of interest with much higher accuracy than the other two methods. The ERGM in particular performed very poorly, achieving accuracy on par with random change in the most challenging settings (Supplementary Figure 2 *bottom right panel*). We hypothesize that the poor performance of the ERGM results from the arbitrary choice of graph statistics used to parameterize the model. As Simpson et al. note in the original ERGM paper, “the most appropriate explanatory metrics vary by network” [52]. Thus, choosing an appropriate set of graph statistics for a given multi-subject connectomics dataset is a highly subjective task, limiting reproducibility of this method across studies. In contrast, the OMNI-based test we propose is a prescriptive statistical procedure that does not require hand tuning for every dataset it is used on.

As it has been previously reported that the BTBR mouse has significant neuroanatomical abnormalities in the corpus callosum [36, 37], we expect our methods to identify this brain region as a strong signal vertex. Our results corroborate this hypothesis: across all mouse strains, the left hemispheric portion corpus callosum is the strongest signal vertex, and its right hemispheric counterpart is the second strongest (note, because this atlas is symmetric, the portions of the corpus callosum in each hemisphere are parcellated as two distinct ROIs) (Supplementary Table 2). In contrast, existing connectomics methods like MDMR fail to identify this salient neurobiological information: as shown in Table 3, MDMR ranks the left corpus callosum as the 34th strongest signal vertex despite its pronounced connective differences across strains. Like other existing graph embedding methods, MDMR does not enjoy the statistical advantages of OMNI, including its interpretability and theoretical foundations.

In Figure 3, we plot the vertex embedding of the corpus callosum obtained by OMNI using a pairs plot [54]. Because OMNI embeds each vertex of the graph in d -dimensional space, the pairs plot allows us to visualize the high-dimensional relationships in this Euclidean representation of network connectivity. Each dot represents the embedded corpus callosum of an individual mouse. These plots show scatter plot matrices on the off-diagonal panels, with kernel density estimates (KDEs) of the marginal distributions (smooth approximations of the underlying distribution of the data) on the diagonal. In the lower triangle of each pairs plot, we show 95% prediction ellipses of the distribution of each strain’s embedding. Together with the KDEs, these figures show a high degree of separability in the embeddings, highlighting the intra-strain heterogeneity of the corpus callosum. Thus, OMNI successfully recovers a distinct representation of the corpus callosum in BTBR mice, and the corroboration of known neurobiological results adds further validation to this approach. For comparison, in Supplementary Figure 5, we also show pairs plots of two weak signal vertices: the left hemisphere cingulate cortex area 29c (rank 170 of 326) and the right hemisphere fasciculus retroflexus (rank 257 of 326). Mice from distinct genotypes are much less separable in embeddings of these vertices compared to the embeddings of the corpus callosum.

Connectomes in this dataset are bilateral (that is, for each region of interest, there is a corresponding structure in both the left and right hemispheres). Therefore, we can aggregate the connective abnormality of a structure across hemispheres, enabling the identification of pairs of vertices that are significant in both the left and right hemisphere. In Supplementary Table 4, we provide a list of the

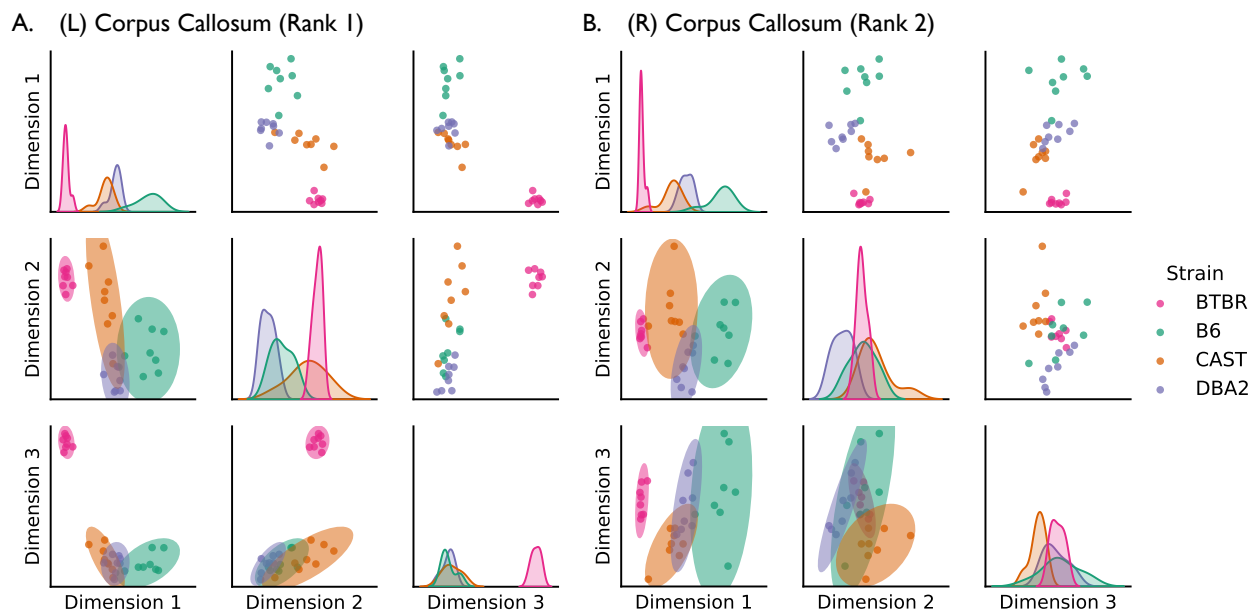


Figure 3: Pairs plots of vertex embedding of the left and right hemisphere corpus callosum produced by the omnibus embedding. The corpus callosum is the bridge between the left and right hemispheres of the brain. In the BTBR mouse, the corpus callosum has highly penetrant neuroanatomical defects; therefore, we expect to differentiate the BTBR mouse from the other strains by examining the embedding of the corpus callosum. We can do this in the embedding of the left hemisphere corpus callosum (the strongest signal vertex) and slightly less clearly in the embedding for the right hemisphere corpus callosum (the second strongest signal vertex). Interestingly, corpus callosum embeddings of wild-type mice are also separable (particularly the B6 strain), suggesting a diversity in corpus callosum architecture across the behavioral controls.

10 strongest signal vertex pairs, which we term bilateral signal vertices. For most bilateral signal vertices, the ROI in one hemisphere is usually a much stronger signal vertex than the other hemisphere (for example, the right hemisphere cerebral peduncle is the 9th ranked signal vertex, while its right hemisphere counterpart is ranked 63rd).

2.3 Interrogating the regional scale

Identifying signal communities Communities of highly interconnected vertices are important structures within connectomes that underlie diverse neurological functions [24, 29]. Therefore, communities are an important topological scale at which connectomes can be analyzed. For analysis of connectomes where vertices are organized using an *a priori* community grouping, we compare four approaches for modelling the connectivity information encoded within a community (see the Methods (§4.4)). Each successive approach yields a more holistic summary of the community. The first two approaches are univariate, comparing either (1) the probability of connectivity in a community or (2) the average edgeweight in a community across populations. While these are fundamental properties of a community, summarizing the behavior of a community with a single scalar loses information. The last two approaches are multivariate, comparing either (3) the indices of nonzero edges in a community or (4) the vector of edgeweights in a community. Note that the operations performed by approaches (1) and (3) require the connectomes to be binarized via Otsu's method [55], whereas approaches (2) and (4) operate on weighted connectomes. To test if the summarized information in a block is different across phenotypes, we again use Dcorr.

We compare these approaches in a two-population simulation setting (see the Methods (§4.7)). All methods were robust to false positives (Supplementary Figure 3 *first panel*), however, they differed in their ability to successfully identify signal communities. In settings where edgeweights in a community

have the same mean but different variances, univariate and binary approaches struggle to identify signal communities, achieving a maximum TPR of 60%. However, comparing multivariate weighted representations of communities proved much more successful with a TPR of 80% for sample sizes $N > 30$ (Supplementary Figure 3 *middle panel*). When edgeweights in a community have different means, all algorithms are able to successfully identify signal communities with a high TPR. However, only the weighted approaches can do this with small sample sizes $N < 25$ (Supplementary Figure 3 *right panel*). Therefore, we propose using Dcorr to compare communities across subjects in *regional scale* analyses.

In Supplementary Figure 4, we show log-transformed p -values obtained by the four approaches described above. Regions in blue are significant at the Holm–Bonferroni correction. Consistent with the simulations in the Methods (§4.7), we see that univariate tests find less signal communities than the multivariate tests. p -values for all communities are given in Supplementary Table 5. The strongest signal community (i.e., the one with the most heterogeneous topology across genotypes) determined by Dcorr is the intraconnection within the right hemisphere white matter. In fact, the majority of the 10 strongest signal communities involve connections to the white matter in both hemispheres.

2.4 Identifying multiscale differences in network architecture across genotypes Using the statistical methods described above, we discover differences in brain connectivity between the four mouse genotypes at each topological scale of the connectome. Figure 4 visualizes the strongest signal edge (as detected by Dcorr), the strongest signal vertex (as detected by OMNI and MANOVA), and the strongest signal community (as detected by Dcorr) using tractograms, renderings of nerve tracts measured in the original DTI data. For an edge, the tractogram represents all the tracts between its two incident vertices; for a vertex, the tractogram represents all the tracts originating from that vertex; and for a community, the tractogram represents all the tracts interconnecting the vertices in a superstructure. A full list of the parameters using to generate these tractograms is available in the Methods (§4.9).

Tractograms allow us to visualize the heterogeneity in brain connectivity identified by our multiscale algorithms. For example, a tractogram of the left corpus callosum (Figure 4 *middle column*) in the BTBR mice reveals a near absence of cross-hemispheric connections, while all control strains display much more cross-hemispheric connections at this vertex. To contrast with these heterogeneous tractograms, Supplementary Figure 6 shows tractograms for the weakest signal edge, vertex, and community. In comparison to the tractograms shown in Figure 4, the tractograms of weak signal components are much more homogeneous across strains. Note, in the calculation of the weakest signal edge, we ignore edges with zero edgeweight for all connectomes.

In addition to tractograms, we also plot the distribution of neurotopological features (edgeweights and embeddings) used to determine the strongest signal structure at each scale (Figure 4 *bottom row*). These distributions highlight the differences in connectome structure that each algorithm used to quantify the signal strength of that specific edge, vertex, or community.

2.5 Interrogating the global scale To complete a multiscale analysis of multi-subject connectomics data, we demonstrate how results from our prior scales of network topology can be aggregated to enable comparisons of patterns in whole-brain connectivity across subjects. OMNI was used to jointly embed every graph in our sample into a low-dimensional subspace. Figure 5A shows the pairwise dissimilarity between each pair of connectomes in our dataset. Pairwise dissimilarity between a pair of connectomes G_1 and G_2 is calculated as the Frobenius norm of the difference between the corresponding embedding of each graph. Note that the dissimilarities in Figure 5A are standardized by dividing by the largest pairwise dissimilarity. The average intra-strain dissimilarity (27%) is smaller than the average inter-strain dissimilarity (67%), confirming that connectomes from mice of the same genotype are globally most similar to one another. Additionally, the BTBR mice are very dissimilar to all other strains (the average inter-strain dissimilarity for the BTBR mice is 79%) while the three control strains are all fairly similar to each other (the average inter-strain dissimilarity for B6, CAST, and DBA2 mice is 55%).

We further reduce the dimensionality of these embeddings by using classical Multidimensional Scal-

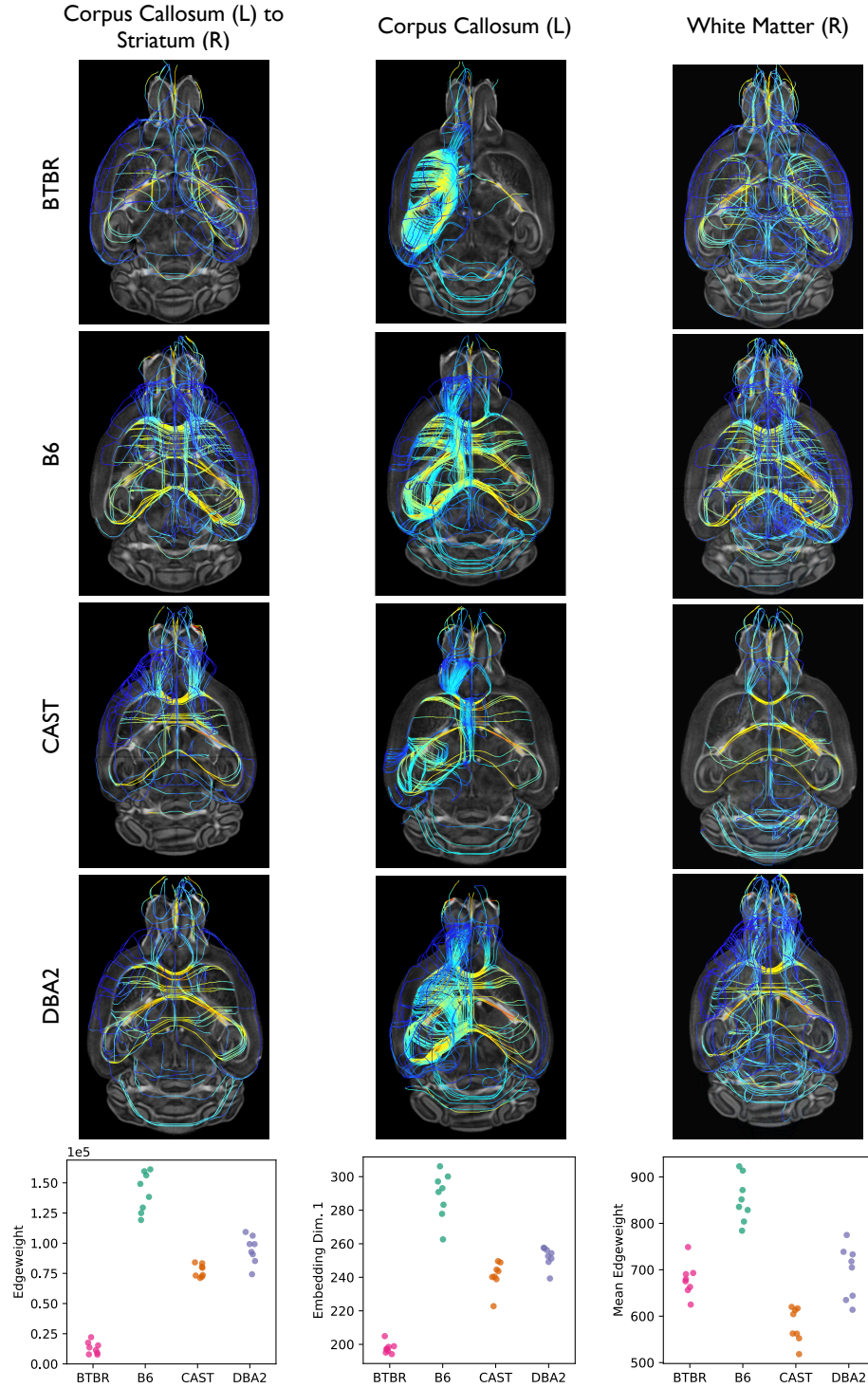


Figure 4: Visualization of the strongest signal edge (left hemisphere corpus callosum to right hemisphere striatum), vertex (left hemisphere corpus callosum), and community (right hemisphere white matter) across all mouse strains. At each topological scale, tractograms of these neurological structures are shown for each mouse strain. (*Bottom row*) The distribution of edgeweights for the strongest signal edge (*Column 1*); the distribution of the first embedding dimension for the strongest signal vertex (*Column 2*); and the distribution of average edgewidth for the strongest signal community (*Column 3*). Each dot represents data from an individual mouse. Connective differences in the left hemisphere corpus callosum are apparent, with BTBR mice displaying a uniformly small vertex embedding. The average edgewidth of the most significant community also shows pronounced variation across strains.

ing (cMDS) to embed this distance matrix into a two-dimensional space [56]. This yields a collection of 32 points in \mathbb{R}^2 , where each point represents the connectome of an individual mouse. The BTBR mice are highly separated from the other three control strains (Figure 5B); all wild-type strains are also clearly distinct from each other (Figure 5C). Thus, we can leverage information from OMNI to successfully differentiate all connectomes based on genotype, enabling comparisons of brain connectivity at the *global scale*.

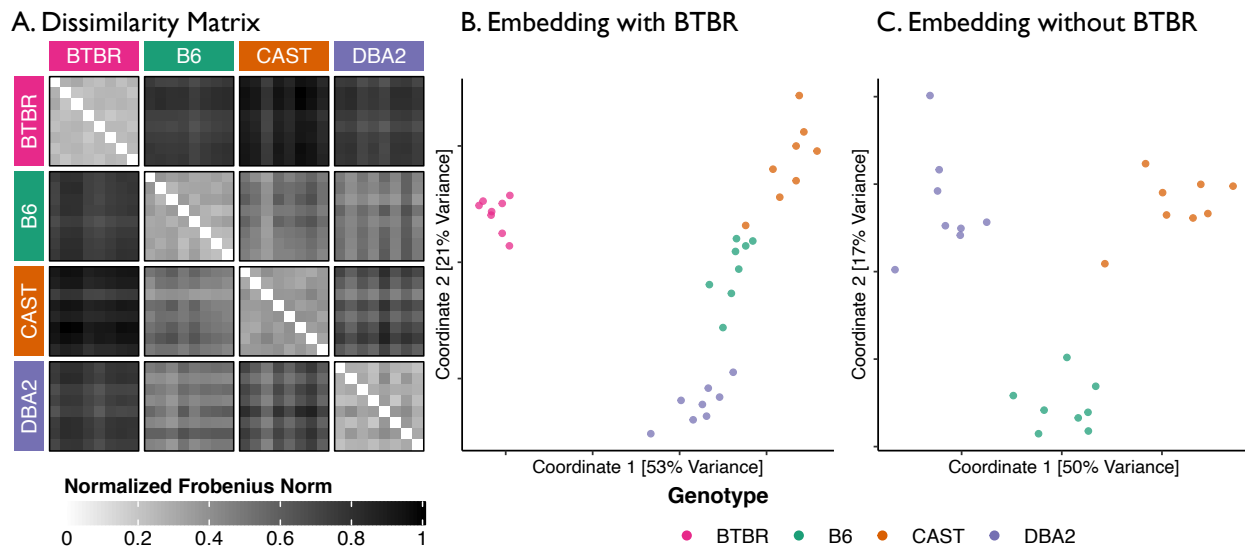


Figure 5: Pairwise distance between each mouse connectome, organized by mouse strain (*left*) and the joint embeddings of each sample with and without connectomes from BTBR mice in a two-dimensional space (*right* and *center*, respectively). Joint embeddings of every connectome were obtained using the omnibus embedding. (*Left*) The pairwise distance between connectomes is calculated as the Frobenius norm of the difference between the embeddings of a pair of connectomes. (*Center*) Two-dimensional representations of each connectome were obtained by using Classical Multidimensional Scaling (cMDS) to reduce the dimensionality of the embeddings obtained by OMNI. (*Right*) Same as center, but without data from BTBR mice. Adapted from [32] with permission.

2.6 The topology of vertices encodes information beyond the anatomy of those vertices Here, we demonstrate that the characterization of vertex-level brain connectivity provided by the omnibus embedding contains topological information that is not available in commonly-used anatomical features. Similar studies have been conducted in functional neuroimaging via connectivity fingerprinting [57, 58], and thus this is an important test to conduct for OMNI. Following registration of all diffusion imaging data, the following anatomical features were derived for each vertex in every mouse brain: volume, apparent diffusion coefficient (ADC), fractional anisotropy (FA), and radial diffusivity (RD). For every vertex, we tested if the genotype labels and the low-dimensional embedding of the vertex produced by OMNI were conditionally independent given any of the anatomical features of that vertex [59]. The implication of this test is that if genotype and the embedding are conditionally independent given a particular feature, then that feature is a confounder [60]. If the alternative is true, then OMNI captures a characterization of brain connectivity (topology) not explained by that anatomical feature. This conditional independence testing procedure is described in further detail in the Methods (§4.8).

We find that for 282 out of 326 vertices, the genotype labels and OMNI embedding were conditionally dependent given each of the anatomical feature (Figure 6). All four anatomical features were confounders for only 28 vertices, and the majority of these vertices were not in the top 100 strongest signal vertices. Thus, for most vertices, the omnibus embedding provides additional insight into connectivity beyond what is explained by the anatomical features, demonstrating the value of this means of *local scale* analysis. Our findings demonstrate that, in most cases, anatomical features do not encode

additional information about mouse genotype than the connectomes.

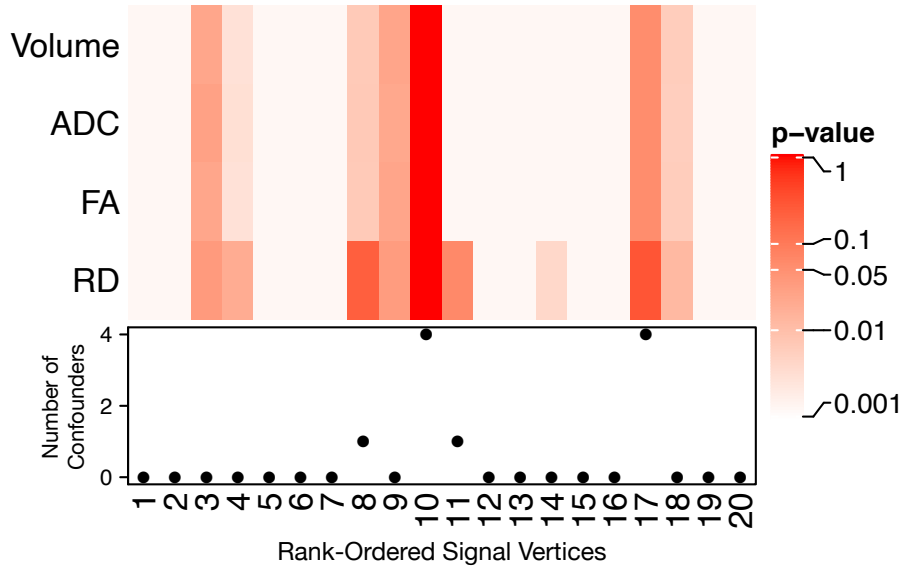


Figure 6: The omnibus embedding provides a novel understanding of brain connectivity at the scale of individual vertices. Using diffusion imaging, the following metrics were measured for each vertex: volume, apparent diffusion coefficient (ADC), fractional anisotropy (FA), and radial diffusivity (RD). To determine if a given feature provided more information than the embedding, these four anatomical features were compared to vertex embeddings produced by OMNI via a conditional independence test. Holm–Bonferroni corrected p -value for each conditional independence test for the top 20 strongest signal vertices (Table 2) are shown on the heatmap above. A cell is red if genotype and the embedding are conditionally independent given the feature, implying that OMNI is confounded by the anatomical feature. The total number of confounding anatomical features for each vertex, sorted by signal strength are shown below the heatmap.

3 Discussion Robust and interpretable statistical methods for analyzing the network topology of connectomes are critically important to understand how patterns in brain connectivity are associated with observable phenotypes. However, in this work, we have shown that many widely-used methods for analyzing connectomes have a host of concerning deficiencies including weak, and often invalid, theoretical foundations (e.g., the T -TEST is not robust for edge-wise testing; Supplementary Figure 1); poor statistical power in simulation settings (e.g., graph statistics provide uninformative descriptions of vertex-level connectivity; Supplementary Figure 2); and an inability to recover obvious neuroanatomical differences in even the simplest connectomics datasets (e.g., Multivariate Distance Matrix Regression (MDMR) fails to identify the corpus callosum as a signal vertex; Table 3). These failings primarily result from the naive application of classical statistical tests to connectomes, which ignores the non-Euclidean topology of network-valued data and underutilizes spatial information encoded in the connectome. The result is a host of methods whose validity is unclear, calling into question the results they produce on real-world

To combat these problems, we leverage recent advances in the theory of random graph models to develop methods that deliver statistically principled and interpretable analyses of multi-phenotype and multi-subject connectomics datasets. Specifically, these methods can be used to identify signal edges, vertices, and communities—that is, the components of the connectome across multiple topological scales that characterize the differences in network architecture observed between samples from distinct phenotypic backgrounds. Additionally, we have formulated these methods as k -sample hypothesis tests, meaning they can be used to jointly analyze connectomes from more than just two dimensional or categorical phenotypes.

The advantages of using random graph models to perform hypothesis tests on connectomes are

numerous:

1. Hierarchical random graph models enable **multiscale modeling** of connectomes;
2. Random graph models are generative, meaning the estimated model parameters characterize the structure of a particular scale of network topology, and are therefore **interpretable**;
3. Unlike many other connectomics methods, random graph models have **provable properties** which motivate robust and principled downstream statistical analyses.

For example, consider the identification of signal vertices using the Random Dot Product Graph (RDPG) and OMNI. A previously demonstrated central limit theorem proved that the embeddings estimated by OMNI are asymptotically normal [51], motivating our use of MANOVA to test for connective differences amongst the ROIs in a connectomics dataset. In contrast, vertex-level graph statistics have no such governing distribution. In fact, multiple studies have shown that connectomes with wildly different topologies can produce identical graph statistics [30, 31] (à la Anscombe’s quartet [61]), so applying classical statistical tests to a set of graph statistics will almost always produce meaningless results. This is reflected in our simulation studies: successfully detecting signal vertices using vertex-level graph statistics is an under-powered statistical approach, with an average area under the ROC curve (AUC) of 68% (Supplementary Figure 2), lagging behind our proposed method, which achieves an average AUC of 87%.

We have previously proposed vertex embedding methods other than OMNI, and while these methods have certain advantages over OMNI in certain scenarios, they too lack many desirable statistical properties. For example, unlike OMNI, the Joint Spectral Embedding [62] can embed connectomes with different numbers of vertices. While this is useful for cross-species comparisons [63], this paradigm is not often encountered in multi-subject connectomics datasets of the same species (e.g., mice or humans) given that the same atlas can be applied to all subjects. One disadvantage of the Joint Spectral Embedding, however, is that its outputs are not interpretable. In OMNI, the embedding of a given vertex (encoded as a vector) quantifies its probability of connecting to any other vertex in the connectome. In addition to lacking such interpretability, the Joint Spectral Embedding does not enjoy the asymptotic properties of OMNI, limiting its application for identifying signal vertices.

Our methods for identifying signal edges, vertices, communities enable powerful multiscale analyses of connectomes. Additionally, we show how information from each of these scales can be aggregated to perform whole-brain comparisons of global scale connectivity (Figure 5). Previous methods have attempted to perform similar multiscale analyses, but, in addition to analyzing fewer scales than our methods are capable of, these previous methods have flawed theoretical foundations. For example, the network based statistic (NBS) aggregates the results from serial edgewise tests to find clusters of inter-connected vertices that are connectively different between two groups [44]. However, NBS uses the T-TEST and arbitrary thresholding to determine which edges in the connectome are signal edges. As we have shown in our simulations, the T-TEST (as well as other tests of location, such as Kruskal–Wallis) performs exceedingly poorly on all but the most well-behaved of edge weight distributions (e.g., two normal distributions with equal variance and different means) (Supplementary Figure 1). Edge weights can be differently distributed across phenotypes, and therefore be true signal edges, but have the same mean (or median), and NBS will fail to successfully identify them as signal edges. To correct for this deficiency, we advocate for the use of DCORR, a nonparametric, universally consistent test for differences in distribution [42, 43]. By treating each edge weight as an independent random variable under the Independent Edge (IE) random graph model, we enable far more powerful edgewise testing. Substituting the T-TEST in NBS with DCORR would be an interesting experiment, however, we could not find a well-validated open-source implementation of NBS with which to test this setup. If one is truly interested in estimating vertex clusters like those produced by NBS, we instead recommend the signal subgraph estimator [27, 64], which has the added benefits of being provably consistent, robust, and interpretable. Open-source Python implementations of the signal subgraph estimator, along with all of our methods, are freely available online [65].

Collectively, the proposed methods presented in this work motivate a number of potential future

extensions. First, there is room to develop statistical innovations that will be able to determine if a particular random graph model appropriately models a given real world dataset. This can be accomplished via tests of goodness-of-fit (GoF), an important criteria for model selection [66]. A GoF test has already been developed for the inhomogeneous Erdős–Rényi random graph [67], a particular version of the $\mathbb{I}\mathbb{E}$ model, and similar tests can be developed for the \mathbb{RDPG} (vertex-level model) and the \mathbb{SBM} (community-level model). Once developed, these tests can be used as a validation step before running any of our proposed multiscale algorithms, adding further rigor to these methods.

Second, while \mathbb{DCORR} enables statistically powerful edge-wise testing, it is very computationally expensive. Performing k -sample testing with \mathbb{DCORR} typically requires a costly permutation test to estimate the null distribution and subsequent p -value. While there is a good chi-square approximation for the null distribution of unbiased \mathbb{DCORR} with comparable finite-sample power [68], this test generally requires a sample size ≥ 20 to be statistically valid. In connectomics, it can sometimes be difficult to achieve a sample this large, particularly if one is studying a rare neurological disorder or using a very time-intensive process to estimate the connectome.

Third, these methods are designed for the comparison of populations of connectomes from distinct categorical or dimensional phenotypes. Statistical modeling of the connectome in relation to a continuous phenotypic variable of interest (such as age) is a fundamental challenge for the analysis of dynamic connectomes. While these methods can be applied if the continuous variable is discretized into categorical bins, extensions are required to enable true regression analysis of the connectome in this statistical modeling framework.

The network-level view of brain organization provided by the connectome will enable a transformative understanding of the brain [69]. For an organ system whose function—both in disease and in health—remains so poorly understood, the promise of this new data type is immense. However, our ability to measure connectomes is quickly outpacing our ability to analyze them. As the wealth of neuroimaging and connectomics data continues to grow, new mathematical and statistical techniques will be required to discover the brain circuits that underlie neurological processes, disorders, and diseases. We anticipate that the multiscale algorithms and techniques presented in this work will be widely used by future researchers to uncover the neurobiological correlates of different phenotypes in multi-subject connectomics datasets.

All statistical methods described in this paper are implemented in `graspologic`, an open-source Python package for statistical network analysis maintained by Microsoft Research (<https://github.com/microsoft/graspologic>). Jupyter Notebooks demonstrating the use of these algorithms on real-world connectomics data are also available in the package’s documentation.

4 Methods

4.1 Correcting for multiple comparisons Connectomes analyzed in comparative multi-subject studies are typically composed of hundreds of vertices and tens of thousands of edges [70]. Therefore, each statistical method we describe in this work performs multiple comparisons on related structures in the connectome. Many standard methods for controlling the false discovery rate such as the Benjamini–Hochberg procedure assume independence, but independence within a network is logically impossible for all but the simplest random graph model (weighted Erdős–Rényi), as each edge is defined specifically by virtue of a dependence between pairs of vertices. In this setting, such methods can result in overly liberal statistical corrections and a high false positive rate [71, 72]. Instead, we use the Holm–Bonferroni correction, a simple and stringent multiple comparison correction that controls the false discovery rate by setting the type 1 error rate (commonly referred to as the *significance level*, α) for each test equal to the original significance level divided by the rank of the p -value corresponding to the test [73]. Like the Bonferroni correction [74], the Holm–Bonferroni correction does not make assumptions that are violated by connectomics data. However, the Holm–Bonferroni correction is uniformly more powerful than the Bonferroni correction [73].

4.2 Graph theory preliminaries Graphs are convenient mathematical objects for representing connectomes. A graph G consists of the tuple (V, E) where V is the set of vertices and E is the set of edges. The set of vertices can be represented as $V = \{1, 2, \dots, n\}$, where $|V| = n$ is the number of vertices. The set of edges is a subset of all possible connections between vertices (i.e., $E \subset V \times V$). We say the tuple $(i, j) \in E$ if there exists an connection from vertex i to vertex j . In many connectomics datasets, edges have associated edge weights: real-valued numbers that encode quantitative information about a connection between two vertices. The interpretation of the edge weight is dependent on imaging modality used to estimate the connectome. For example, the edge weight in human structural connectomes are non-negative integers that represent the number of estimated neuronal fibers that traverse from one region of the brain to another [75]. Every connectome has an associated weighted adjacency matrix $\mathbf{A} \in \mathbb{R}^{n \times n}$ where \mathbf{A}_{ij} denotes the weight of the edge $(i, j) \in E$.

4.3 Random graph models Statistical modeling of connectomics data enables the principled analysis of these high-dimensional, graph-valued data. Random graph models treat individual connectomes as random variables, enabling mathematical characterization of network structure and accounting for noise within and across observed samples. Below, we present three such models: 1) the Independent Edge (IE) model; 2) the Random Dot Product Graph (RDPG); and 3) the Stochastic Block Model (SBM). Each model is designed to characterize a particular topological scale of a network, either its edges, vertices, or communities. This network modelling approach enables the formulation of inferential statistical hypothesis tests that can be used to identify connective differences at specific scales across multiple phenotypes.

The edge model In the Independent Edge (IE) model, every possible edge in the connectome $(i, j) \in V \times V$ occurs with some probability $p_{ij} \in [0, 1]$. We construct a matrix of probabilities $\mathbf{P} \in [0, 1]^{n \times n}$, where $\mathbf{P}_{ij} = p_{ij}$. Thus, a graph is given by the model $G \sim \text{IE}(\mathbf{P})$ if its adjacency matrix \mathbf{A} has entries $\mathbf{A}_{ij} \sim \text{Bernoulli}(p_{ij})$ for all $(i, j) \in V \times V$. In the analytical methods presented in the Methods (§4.4), we consider the weighted IE model to account for a network with weighted edges. For this variant, instead of sampling a binary edge from $\text{Bernoulli}(p_{ij})$, we sample each edge weight from a distribution F_{ij} . In this setting, \mathbf{P} represents a matrix of univariate probability distribution functions for the weight of each edge in the connectome. When estimating the \mathbf{P} matrix for a weighted IE graph, it is typical to assume that all elements of \mathbf{P} are from the same family of distributions.

The vertex model The Random Dot Product Graph (RDPG) is a generalization of the IE model that belongs to the family of latent position random graphs [76]. In certain scenarios, the probability of a connection p_{ij} may not be directly observable. Instead, each vertex is associated with a *latent position* x_i , which is a member of some space \mathcal{X} . The probability of a connection between vertices i and j is given by a link function $\kappa : \mathcal{X} \times \mathcal{X} \mapsto [0, 1]$; that is, $p_{ij} = \kappa(x_i, x_j)$. In the RDPG, the latent space \mathcal{X} is a subspace of Euclidean space \mathbb{R}^d and the link function is the dot product [77]. Thus, in a d -dimensional RDPG with n vertices, the rows of the matrix $\mathbf{X} \in \mathbb{R}^{n \times d}$ encode the latent position of each vertex, and the matrix of connection probabilities is given by $\mathbf{P} = \mathbf{X}\mathbf{X}^\top$. A graph is sampled the model $G \sim \text{RDPG}(\mathbf{X})$ if its adjacency matrix \mathbf{A} has entries $\mathbf{A}_{ij} \sim \text{Bernoulli}(\langle x_i, x_j \rangle)$ for $(i, j) \in V \times V$.

The community model In the Stochastic Block Model (SBM), every vertex belongs to one of K communities, which are disjoint subsets of the vertex set V [78]. The SBM is a special case of the RDPG in which all vertices from the same community have identical latent positions; that is, the connection probability is solely determined by community membership. A symmetric $K \times K$ community connectivity probability matrix \mathbf{B} with entries in $[0, 1]^{K \times K}$ governs the probability of an edge between vertices given their community memberships. Community membership is determined by the vertex assignment vector $\vec{\tau} \in \{1, \dots, K\}^n$, which is either unknown or given *a priori*. Because brain regions in our dataset are hierarchically grouped into superstructures and hemispheres, we assume that $\vec{\tau}$ is given. Thus, a graph is sampled the model $G \sim \text{SBM}(\mathbf{B})$ with $\vec{\tau}$ given if its adjacency matrix \mathbf{A} has entries $\mathbf{A}_{ij} \sim \text{Bernoulli}(\mathbf{B}_{kl})$ where $\tau_i = k, \tau_j = l$, for $(i, j) \in V \times V$, and $k, l \in \{1, \dots, K\} \times \{1, \dots, K\}$. As with the IE model, a weighted variant of the SBM can be constructed by replacing the

block probability \mathbf{B}_{ij} with a probability distribution function F_{ij} for the entire block.

In our simulations, we will consider two variations of the two-community Sbm ($K = 2$) with block connectivity matrix $\mathbf{B} = \begin{bmatrix} a & b \\ c & d \end{bmatrix}$, abbreviated as $\mathbf{B} = [a, b; c, d]$. These include:

1. Planted Partition: $a = d$ and $b = c$. In this model, the within-community edges share a common probability a , and the between-community edges share a common probability b , where $a \neq b$.
2. Symmetric Heterogeneous: $b = c$. In this model, the between-block edges share a common probability b , but the within-block edges have a disparate probabilities, where $a \neq b \neq d$.

4.4 Formulations of statistical methods for multiscale inference

Identifying signal edges Univariate edge-wise testing provides an interpretable and simple computational approach for identifying relationships between specific edges and phenotypes. Using the IE model, we assume that each connectome is sampled from a phenotype-conditional probability matrix; that is, we assume that for each phenotype in \mathcal{Y} , there is an associated probability matrix in $\{\mathbf{P}^{c_1}, \dots, \mathbf{P}^{c_k}\}$ from which all connectomes in that phenotype are sampled. For a given edge (i, j) , we assume the edge weight for each connectome has been independently and identically (i.i.d) sampled from the appropriate \mathbf{P} matrix. Specifically, we assume that for every connectome in phenotype $c_i \in \mathcal{Y}$, the edge weight $\mathbf{A}_{ij} \sim \mathbf{P}_{ij}^{c_i}$ i.i.d. Following this assumption, we formulate the following null and alternative hypotheses:

$$\begin{aligned} H_0 : \forall(y, y') : \quad & \mathbf{P}_{ij}^{c_y} = \mathbf{P}_{ij}^{c_{y'}} \\ H_A : \exists(y, y') : \quad & \mathbf{P}_{ij}^{c_y} \neq \mathbf{P}_{ij}^{c_{y'}} \end{aligned}$$

To test the null hypothesis, any univariate statistical test can be employed at each potential edge $e \in E$. We use a one-sided k -sample test of distance correlation (DCORR) to determine if the distribution of an edge weight differs across populations. In the Methods (§4.5), we demonstrate that DCORR is a more powerful test than common non-parametric and Gaussian alternatives. Additionally, serial edge-wise testing requires corrections for an immense number of multiple comparisons. If the sample consists of directed graphs, then the total number of tests is n^2 ; if the graphs are undirected, then the total number of tests is $\binom{n}{2}$.

Identifying signal vertices A sample of connectomes can be jointly embedded in a low-dimensional Euclidean space using the omnibus embedding (OMNI). A host of machine learning tasks can be accomplished with this joint embedded representation of the connectome, such as clustering or classification of vertices. Here, we use the embedding to formulate a statistical test that can be used to identify vertices that are strongly associated with given phenotypes.

For each graph in the population, OMNI jointly maps each vertex $v \in V$ to a vector $x_i \in \mathbb{R}^d$ that corresponds to the vertex's latent position in a d -dimensional RDPG . According to a Central Limit Theorem for OMNI , these latent positions are universally consistent and asymptotically normal [51]. This motivates our use of normal-theory inferential statistical tests to determine if the embedding of a given vertex is different across phenotypes. If the number of classes $k = 2$, we use Hotelling's T-squared (HOTELLING'S), a multivariate generalization of the T-TEST ; if $k > 2$, we use one-way MANOVA with the Pillai trace as our test statistic. We formulate the following null and alternative hypotheses:

$$\begin{aligned} H_0 : \forall(y, y') : \quad & \mu_{c_y} = \mu_{c_{y'}} \\ H_A : \exists(y, y') : \quad & \mu_{c_y} \neq \mu_{c_{y'}} \end{aligned}$$

where μ_{c_i} is the mean latent position for the phenotype $c_i \in \mathcal{Y}$. This procedure results in n statistical tests (one for each vertex).

Identifying signal communities Vertices in a connectome can be hierarchically organized into superstructures such as major brain regions and hemispheres. The interactions within and between these

communities of vertices form connective circuits within the brain, and are more correlated with complex behavior and phenotypes than single edges or vertices. Therefore, interrogation of the *regional scale* and identification of signal communities is critical component of multiscale connectomics analysis.

Here, we use the SBM to model the community structure of a connectome. We propose four approaches for describing the connectivity of a community, and an accompanying statistical procedure for each approach. Each subsequent approach provides a more holistic description of a community. For a given community (i, j) and for each phenotype, we do the following:

1. Average Connectivity: Compute the average number of nonzero edges (binarize using Otsu's method [55]), which is equivalent to the community connectivity probability B_{ij} . We then use Pearson's chi-squared to determine if there is a significant difference in the connectivity probability across phenotypes.
2. Average Edge Weight: Compute the average weight of all the edges, essentially treating the community as a single large edge. We then use Dcorr to determine if there is a significant difference in the average edge weight across phenotypes.
3. Multivariate Binary: Binarize the community using Otsu's method [55], and vectorize the subgraph of the adjacency matrix corresponding to that community. We binarize to determine if the distribution of nonzero edges is different across phenotypes. Test for differences in this binary representation using Dcorr.
4. Multivariate Weighted: Vectorize the subgraph of the adjacency matrix corresponding to that community. Again, test for differences in this weighted representation using Dcorr.

In the Methods (§4.7), we demonstrate via simulations that the Multivariate Weighted method is superior to the other three. If the connectomes in question have b communities and are directed, this procedure results in b^2 comparisons. If the connectomes are undirected, this procedure results in $\binom{b}{2}$ comparisons.

4.5 Edge simulations We consider two populations of networks generated from a two-community SBM. Edge weights are sampled from a truncated normal distribution to emulate correlation matrices. All networks have $n = 20$ vertices with 10 vertices belonging to the first community and 10 vertices belonging to the second community. The community probability matrix for each population is given by

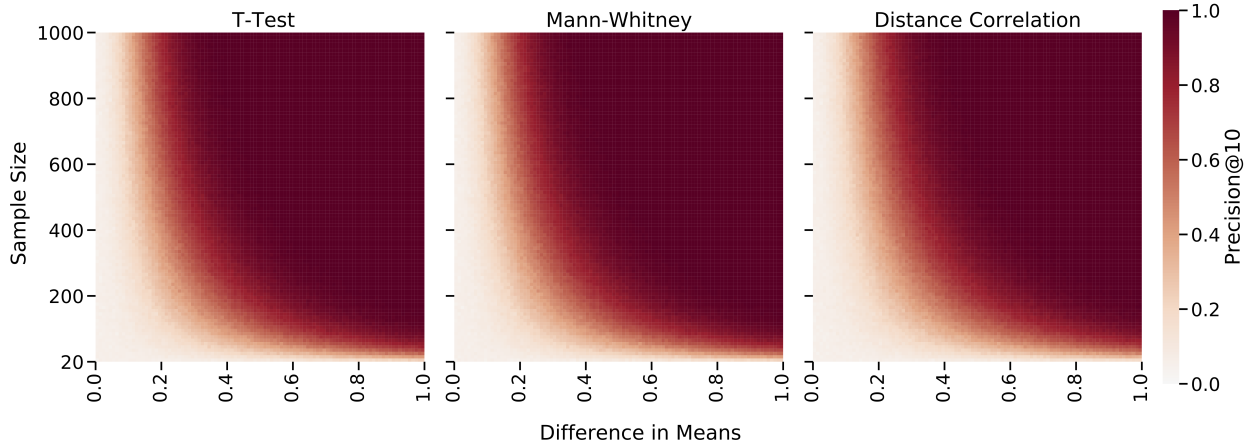
$$\mathbf{B}^1 = \begin{bmatrix} \mathcal{TN}(0, 0.25) & \mathcal{TN}(0, 0.25) \\ \mathcal{TN}(0, 0.25) & \mathcal{TN}(0, 0.25) \end{bmatrix}$$

$$\mathbf{B}^2 = \begin{bmatrix} \mathcal{TN}(0 + \delta, 0.25 + \phi) & \mathcal{TN}(0, 0.25) \\ \mathcal{TN}(0, 0.25) & \mathcal{TN}(0, 0.25) \end{bmatrix}$$

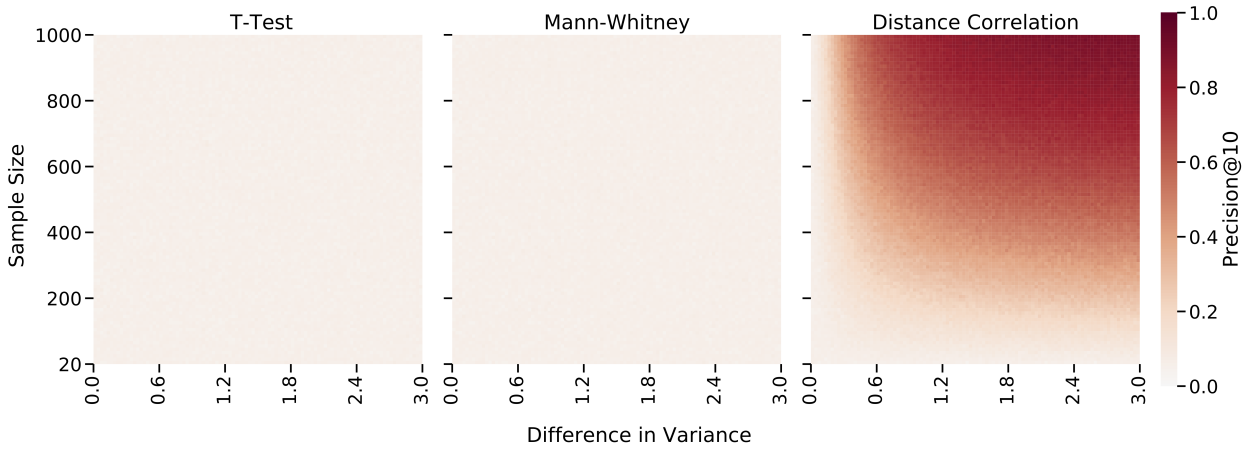
where $\mathcal{TN}(\mu, \sigma^2)$ denotes a truncated normal distribution with mean μ and variance σ^2 such that all values are bounded within $[-1, 1]$. A total of $m = 20, 40, \dots, 1000$ networks are sampled ($m/2$ networks per population). In the first population, all edges are sampled from the same edge weight distribution $\mathcal{TN}(0, 0.25)$. In the second population, all edge weights are also sampled from $\mathcal{TN}(0, 0.25)$ except for those in the first community. In this community, the distribution of edge weights has either a different mean, δ , or variance, $0.25 + \phi$, from the first population. Therefore, the edges in the first community of these simulated connectomes are the signal edges that we hope to correctly identify. For each edge, p -values are computed by three different tests: 1) T-TEST, 2) Mann-Whitney (MW) U test, a non-parametric test of medians, and 3) 2-sample Distance Correlation (Dcorr) test, a test of equality in distribution. For each test, the p -values are sorted to find the ten most significant edges, and the performance is evaluated with precision (the number of signal edges that are correctly identified).

Supplementary Figure 1 shows the Precision@10 as a function of sample size, mean, and variance. Supplementary Figure 1 top row shows that all three tests can identify signal edges that are different in mean, and that no particular test is superior than another in this setting. Supplementary Figure 1 bottom row shows that only Dcorr can detect signal edges with differences in variance when the means are kept the same. This is because T-TEST and MW test for differences in location (e.g. mean or median), whereas Dcorr tests for any differences between a pair of observed distributions. Because

A. Setting 1: Varying Signal Edge Mean



B. Setting 2: Varying Signal Edge Variance

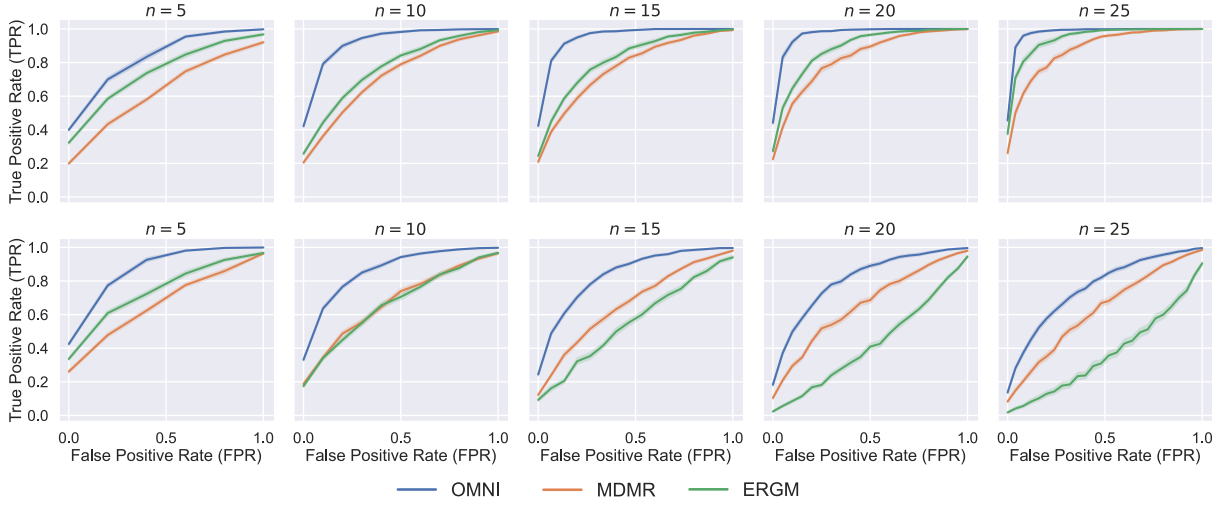


Supplementary Figure 1: Precision@10 for each edge when comparing two populations of weighted networks using the T-TEST, Mann-Whitney U test, and k -sample Dcorr test. The color bar represents precision averaged over 100 trials. (*Top row*) Results for varying the mean δ and sample size while keeping the variance constant ($\phi = 0$). In this setting, all three tests perform similarly, and can detect signal edges when edge distributions differ in means. (*Bottom row*) Results for varying the variance ϕ and sample size while keeping the mean constant ($\delta = 0$). T-TEST and Mann-Whitney test cannot detect changes in variance regardless of the sample and effect size. k -sample Dcorr test is the only test that can detect signal edges with changes in variance.

Dcorr achieves about the same precision and recall as the location tests when only location varies, and demonstrates considerably better operating characteristics when the variance varies, we use it in the real-world data. Note that when looking at the top- k edges, the choice of k is arbitrary. The salient point from this simulation is that if we look at the top-10 edges identified by each algorithm, none of those edges selected by the T-TEST and MW are signal edges — on average, they are false positives.

If the sample size $m \geq 20$, one can use a chi-square test that well approximates the k -sample Dcorr test [68]. This can improve the computational efficiency of edge-wise testing by avoiding the costly permutation test that Dcorr normally uses to estimate the null distribution.

4.6 Vertex simulations One goal of connectomics is to identify signal vertices that are different between populations. In this section, we identify signal vertices using different vector-based vertex representations. The first representation we consider is the simplest: it is possible describe a vertex using all its incident edges via the corresponding row (or column) of a vertex in the adjacency ma-



Supplementary Figure 2: Ability of various vertex representations to identify signal vertices. The number of vertices in each network is kept constant (50), but the number of signal vertices is changed ($n = 5, 10, 15, 20, 25$). For each vertex, we compute a p -value from each of the three vertex representations using `HOTELLING`'s, and set the significance level at $\alpha = 0.05$ following Holm–Bonferroni correction. Colors correspond to the method of vertex representation. (*Top row*) This setting compares two different RDPGs where the perturbed latent position is stretched by a constant. (*Bottom row*) This setting compares RDPGs where the perturbed latent position is rotated and stretched by a constant. Both settings show that OMNI successfully differentiates null and signal vertices with much more accuracy than either MDMR or the ERGM.

trices, and compare these vectors using Multivariate Distance Matrix Regression (MDMR) [53]. The second representation we consider, which is highly popular in modern connectomics literature, is a set of vertex-level graph statistics. Specifically, we fit an exponential random graph model (ERGM) [52] with the following graph statistics for each vertex: local clustering coefficient (LCC), betweenness centrality (BC), closeness centrality (CC), and number of triangles. The final representation we consider are the low-dimensional latent-space positions estimated by OMNI. Since all vertex representations are multivariate, hypotheses are tested using `HOTELLING`'s test, a multivariate generalization of the `T-TEST`.

We consider a population of RDPGs in two different settings where the number of signal vertices is varied. In both settings, m null vertices are sampled from the latent position $X_1 = [0.25, 0.25]$ and n signal vertices are sampled from $X_2 = \text{rot}(70^\circ)X_1$, where $\text{rot}(\theta)$ represents a 2-dimensional rotation matrix of angle θ . In setting 1, X_2 is stretched, and a second RDPG is constructed with latent positions X_1 and $X_3 = 0.4X_2$ and an equivalent number of vertices per each position. In setting 2, X_2 is stretched and rotated (i.e., $X_3 = 0.4\text{rot}(10^\circ)X_2$). The vertices sampled from X_2 or X_3 (i.e., from different latent positions) are considered signal vertices, and we vary the number of these vertices from $n = 0, 5, 10, 15, 20, 25$. The number of null vertices is set to $m = 50 - n$. A total of 100 networks are sampled per population, and the p -values are computed using `HOTELLING`'s on each of the three vertex representations for each vertex. Vertices with p -values less than $\alpha = 0.05$ after Holm–Bonferroni correction are classified as signal vertices in this simulation. The performance of each algorithm is measured using a Receiver Operator Characteristic (ROC) curve, which shows the trade-off between the False Positive Rate and True Positive Rate for each method.

Supplementary Figure 2 shows that OMNI is uniformly a more accurate method for identifying signal vertices. Across all settings, its accuracy (measured by the Area Under the ROC curve) is higher than the other two methods. In particular, the ERGM, which uses the widely popular approach of graph statistics, performs much worse.

4.7 Community simulations We consider two populations of networks generated from a three-community block diagonal SBM. As in the edge simulation (Methods §4.5), edge weights are sampled from truncated normal distributions to emulate correlation matrices. All communities have $n = 10$ vertices each, and the community probability matrix for each population is given by

$$\mathbf{B}^1 = \begin{bmatrix} \mathcal{TN}(0, 0.25) & & \\ & \mathcal{TN}(0, 0.25) & \\ & & \mathcal{TN}(-0.75, 0.25) \end{bmatrix}, \text{ and}$$

$$\mathbf{B}^2 = \begin{bmatrix} \mathcal{TN}(0, 0.25) & & \\ & \mathcal{TN}(0, 0.50) & \\ & & \mathcal{TN}(0.75, 0.25) \end{bmatrix}.$$

A total of $m = 10, 20, \dots, 100$ networks are sampled ($m/2$ networks per population). Note that the edge weight distributions in the first diagonal block are equal, while the distributions have different variances in the second diagonal block and different means in the third diagonal block. Therefore, data from block one allow us to measure the false positive rate (FPR), while data from blocks two and three allow us to measure the true positive rate (TPR). Each simulation run was conducted 50 times to ensure accurate estimation of the FPR and TPR. All p -values were corrected using Holm–Bonferroni with significance determined at $\alpha = 0.05$.

From these simulations, we see that all four tests have roughly the same FPR (about 5% regardless of sample size) (Supplementary Figure 3 *first panel*). However, they differ in their ability to detect signal communities. When all populations have the same mean edge weight, but different variances, only the Multivariate Weighted method consistently detects signal communities once the sample size is greater than 25 networks (Supplementary Figure 3 *second panel*). All other methods have a lower TPR in this setting. When the edge weights have different means, the TPR of the Multivariate Weighted method lags behind the Average Edge Weight method in low sample size settings ($N < 25$) (Supplementary Figure 3 *third panel*). However, when the sample size is larger than $N > 25$, the Multivariate Weighted and Average Edge Weight methods perform comparably. These simulations demonstrate that the Multivariate Weighted signal community detection method, which includes the most information about connectivity within a block, achieves the highest TPR while maintaining a FPR less than or equal to the significance value of the test.

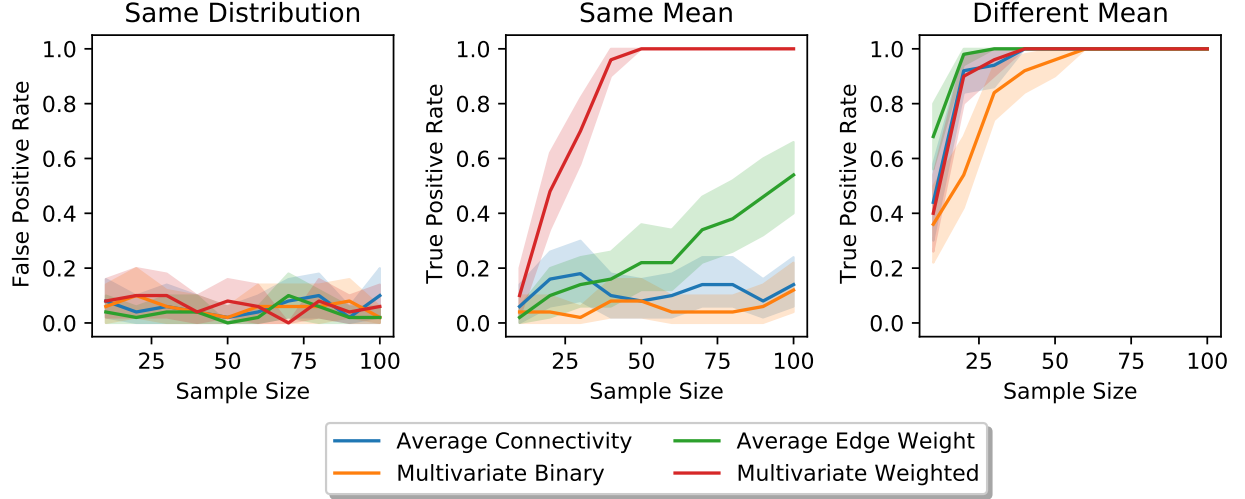
4.8 Conditional independence testing Let $Y \in \mathcal{Y}$ be a random variable representing the genotype of a mouse. For a given vertex i , let $X \in \mathcal{X}$ be a random variable representing the vertex’s latent position in a RDPG estimated by OMNI. Additionally, let vertex i be described by a vector of anatomical features (denoted $A \in \mathcal{A}$) measured from raw neuroimaging data. We are interested in relatively how much signal about genotype is encoded in X and A , respectively.

We can do this using an conditional independence testing framework. If genotype and the embedding are conditionally independent given the anatomical features, then the following is true:

$$(Y \perp\!\!\!\perp X) \mid A \implies \Pr(Y \mid X, A) = \Pr(Y \mid A).$$

That is, the information about connectivity encoded in the vertex’s latent position is redundant given the anatomical features. However, if null hypothesis of conditional independence is rejected, the latent position contains information about connectivity not represented in the anatomy.

4.9 Tractography Deterministic tractograms were generated in DST Studio using the generalized Q-sampling fiber tracking algorithm [79]. For the specific parameter values used for tract generation, see §2.6 of [32]. A group average template was constructed from the 4 male mice per strain. A DTI diffusion scheme was used, and a total of 46 diffusion sampling directions were acquired. The b-value was 4000 s/mm². The in-plane resolution and the slice thickness were both 0.045 mm. The diffusion data were reconstructed in the MNI space using q-space diffeomorphic reconstruction [80] to obtain the spin distribution function [81]. A diffusion sampling length ratio of 1.25 was used. The restricted diffusion was quantified using restricted diffusion imaging [82].



Supplementary Figure 3: The Multivariate Weighted approach for signal community detection is superior to other proposed methods. We consider a two-population simulation where edge weights are sampled from 3-community block diagonal SBM. Distributions in the first block are equal, allowing us to measure the False Positive Rate for each method. We see that all methods achieve a FPR less than or equal to α (*left panel*). In the second block, the two distributions have the same mean, but different variances. The Multivariate Weighted method is the most able to detect community edges in this setting, however it requires a sample size of at least $N = 25$ (*middle panel*). In the third block, the two distributions have different means, and in this setting, the Average Edge Weight method is superior given small sample sizes ($N < 25$) (*right panel*). However, when the samples size is sufficiently large, the Multivariate Weighted method is equivalent. These results demonstrate the superiority of the Multivariate Weighted method over other proposed methods.

5 Data availability Mouse connectomes were derived by Wang et al. and are described in further detail in the original publication [32]. These data are freely available in *graspologic* (<https://github.com/microsoft/graspologic/>) [65], an open-source Python package for statistical graph analysis.

6 Code availability All graph-related simulations and analyses were performed using *graspologic* (<https://github.com/microsoft/graspologic/>) [65] and all multivariate hypothesis testing was performed using *hyppo* (<https://github.com/neurodata/hyppo>) [43]. Heatmaps were generated using *ComplexHeatmap* [83]. The documentation and code for all analyses in this work are available at: <https://github.com/neurodata/MCC.git>.

7 Acknowledgements This work was supported by funding from Microsoft Research, NIH 1RF1MH121539-01, and R01 AG066184/AG/NIA NIH HHS/United States.

References

- [1] Russell A. Poldrack. Can cognitive processes be inferred from neuroimaging data? *Trends in Cognitive Sciences*, 10(2):59–63, February 2006. ISSN 13646613. doi: 10.1016/j.tics.2005.12.004.
- [2] Karl Magnus Petersson, Alexandra Reis, and Martin Ingvar. Cognitive processing in literate and illiterate subjects: A review of some recent behavioral and functional neuroimaging data. *Scandinavian Journal of Psychology*, 42(3):251–267, July 2001. ISSN 0036-5564, 1467-9450. doi: 10.1111/1467-9450.00235.
- [3] Susan R. Hintz, Patrick D. Barnes, Dorothy Bulas, Thomas L. Slovis, Neil N. Finer, Lisa A. Wrage, Abhik Das, Jon E. Tyson, David K. Stevenson, Waldemar A. Carlo, Michele C. Walsh, Abbot R. Laptook, Bradley A. Yoder, Krisa P. Van Meurs, Roger G. Faix, Wade Rich, Nancy S. Newman, Helen Cheng, Roy J. Heyne, Betty R. Vohr, Michael J. Acarregui, Yvonne E. Vaucher, Athina Pappas, Myriam Peralta-Carcelen, Deanne E. Wilson-Costello, Patricia W. Evans, Ricki F. Goldstein, Gary J. Myers, Brenda B. Poindexter, Elisabeth C. McGowan, Ira Adams-Chapman, Janell Fuller, Rosemary D. Higgins, and for the SUPPORT Study Group of the Eunice Kennedy Shriver National Institute of Child Health and Human Development Neonatal Research Network. Neuroimaging and Neurodevelopmental Outcome in Extremely Preterm Infants. *Pediatrics*, 135(1):e32–e42, January 2015. ISSN 0031-4005, 1098-4275. doi: 10.1542/peds.2014-0898.
- [4] Chaim Huyser, Dick J. Veltman, Else de Haan, and Frits Boer. Paediatric obsessive–compulsive disorder, a neurodevelopmental disorder? *Neuroscience & Biobehavioral Reviews*, 33(6):818–830, June 2009. ISSN 01497634. doi: 10.1016/j.neubiorev.2009.01.003.
- [5] Theodore D. Satterthwaite, Mark A. Elliott, Kosha Ruparel, James Loughhead, Karthik Prabhakaran, Monica E. Calkins, Ryan Hopson, Chad Jackson, Jack Keefe, Marisa Riley, Frank D. Mentch, Patrick Sleiman, Ragini Verma, Christos Davatzikos, Hakon Hakonarson, Ruben C. Gur, and Raquel E. Gur. Neuroimaging of the Philadelphia Neurodevelopmental Cohort. *NeuroImage*, 86:544–553, February 2014. ISSN 10538119. doi: 10.1016/j.neuroimage.2013.07.064.
- [6] Habib Ganjgahi, Anderson M. Winkler, David C. Glahn, John Blangero, Peter Kochunov, and Thomas E. Nichols. Fast and powerful heritability inference for family-based neuroimaging studies. *NeuroImage*, 115:256–268, July 2015. ISSN 10538119. doi: 10.1016/j.neuroimage.2015.03.005.
- [7] Kai-Kai Shen, Stephen Rose, Jurgen Fripp, Katie L. McMahon, Greig I. de Zubicaray, Nicholas G. Martin, Paul M. Thompson, Margaret J. Wright, and Olivier Salvado. Investigating brain connectivity heritability in a twin study using diffusion imaging data. *NeuroImage*, 100:628–641, October 2014. ISSN 10538119. doi: 10.1016/j.neuroimage.2014.06.041.
- [8] Peter Kochunov, Neda Jahanshad, Daniel Marcus, Anderson Winkler, Emma Sprooten, Thomas E. Nichols, Susan N. Wright, L. Elliot Hong, Binish Patel, Timothy Behrens, Saad Jbabdi, Jesper Andersson, Christophe Lenglet, Essa Yacoub, Steen Moeller, Eddie Auerbach, Kamil Ugurbil, Stamatis N. Sotiropoulos, Rachel M. Brouwer, Bennett Landman, Hervé Lemaitre, Anouk den Braber, Marcel P. Zwiers, Stuart Ritchie, Kimm van Hulzen, Laura Almasy, Joanne Curran, Greig I. deZubicaray, Ravi Duggirala, Peter Fox, Nicholas G. Martin, Katie L. McMahon, Braxton Mitchell, Rene L. Olvera, Charles Peterson, John Starr, Jessika Sussmann, Joanna Wardlaw, Margie Wright, Dorret I. Boomsma, Rene Kahn, Eco J.C. de Geus, Douglas E. Williamson, Ahmad Hariri, Dennis van 't Ent, Mark E. Bastin, Andrew McIntosh, Ian J. Deary, Hilleke E. Hulshoff pol, John Blangero, Paul M. Thompson, David C. Glahn, and David C. Van Essen. Heritability of fractional anisotropy in human white matter: A comparison of Human Connectome Project and ENIGMA-DTI data. *NeuroImage*, 111:300–311, May 2015. ISSN 10538119. doi: 10.1016/j.neuroimage.2015.02.050.
- [9] Rongjian Li, Wenlu Zhang, Heung-Il Suk, Li Wang, Jiang Li, Dinggang Shen, and Shuiwang Ji. Deep Learning Based Imaging Data Completion for Improved Brain Disease Diagnosis. In Polina Golland, Nobuhiko Hata, Christian Barillot, Joachim Hornegger, and Robert Howe, editors, *Medical Image Computing and Computer-Assisted Intervention – MICCAI 2014*, volume 8675, pages 305–

312. Springer International Publishing, Cham, 2014. ISBN 978-3-319-10442-3 978-3-319-10443-0. doi: 10.1007/978-3-319-10443-0_39.
- [10] Phoebe Spetsieris, Yilong Ma, Shichun Peng, Ji Hyun Ko, Vijay Dhawan, Chris C. Tang, and David Eidelberg. Identification of Disease-related Spatial Covariance Patterns using Neuroimaging Data. *Journal of Visualized Experiments*, 76:50319, June 2013. ISSN 1940-087X. doi: 10.3791/50319.
 - [11] Alessia Sarica, Antonio Cerasa, and Aldo Quattrone. Random Forest Algorithm for the Classification of Neuroimaging Data in Alzheimer’s Disease: A Systematic Review. *Frontiers in Aging Neuroscience*, 9:329, October 2017. ISSN 1663-4365. doi: 10.3389/fnagi.2017.00329.
 - [12] the Alzheimer’s Disease Neuroimaging Initiative, Christian Habeck, and Yaakov Stern. Multivariate Data Analysis for Neuroimaging Data: Overview and Application to Alzheimer’s Disease. *Cell Biochemistry and Biophysics*, 58(2):53–67, November 2010. ISSN 1085-9195, 1559-0283. doi: 10.1007/s12013-010-9093-0.
 - [13] Ed Bullmore and Olaf Sporns. Complex brain networks: Graph theoretical analysis of structural and functional systems. *Nature Reviews Neuroscience*, 10(3):186–198, March 2009. ISSN 1471-003X, 1471-0048. doi: 10.1038/nrn2575.
 - [14] Sebastiano Galantucci, Federica Agosta, Elka Stefanova, Silvia Basaia, Martijn P. van den Heuvel, Tanja Stojković, Elisa Canu, Iva Stanković, Vladana Spica, Massimiliano Copetti, Delia Gagliardi, Vladimir S. Kostić, and Massimo Filippi. Structural Brain Connectome and Cognitive Impairment in Parkinson Disease. *Radiology*, 283(2):515–525, May 2017. ISSN 0033-8419, 1527-1315. doi: 10.1148/radiol.2016160274.
 - [15] Hannelore Aerts, Wim Fias, Karen Caeyenberghs, and Daniele Marinazzo. Brain networks under attack: Robustness properties and the impact of lesions. *Brain*, 139(12):3063–3083, December 2016. ISSN 0006-8950, 1460-2156. doi: 10.1093/brain/aww194.
 - [16] Gyujoon Hwang, Bruce Hermann, Veena A. Nair, Lisa L. Conant, Kevin Dabbs, Jed Mathis, Cole J. Cook, Charlene N. Rivera-Bonet, Rosaleena Mohanty, Gengyan Zhao, Dace N. Almane, Andrew Nencka, Elizabeth Felton, Aaron F. Struck, Rasmus Birn, Rama Maganti, Colin J. Humphries, Manoj Raghavan, Edgar A. DeYoe, Barbara B. Bendlin, Vivek Prabhakaran, Jeffrey R. Binder, and Mary E. Meyerand. Brain aging in temporal lobe epilepsy: Chronological, structural, and functional. *NeuroImage: Clinical*, 25:102183, 2020. ISSN 22131582. doi: 10.1016/j.nicl.2020.102183.
 - [17] Oscar Miranda-Dominguez, Eric Feczko, David S. Grayson, Hasse Walum, Joel T. Nigg, and Damien A. Fair. Heritability of the human connectome: A connectotyping study. *Network Neuroscience*, 2(2):175–199, June 2018. ISSN 2472-1751. doi: 10.1162/netn_a_00029.
 - [18] Edward T. Bullmore and Danielle S. Bassett. Brain Graphs: Graphical Models of the Human Brain Connectome. *Annual Review of Clinical Psychology*, 7(1):113–140, April 2011. ISSN 1548-5943, 1548-5951. doi: 10.1146/annurev-clinpsy-040510-143934.
 - [19] R Cameron Craddock, Saad Jbabdi, Chao-Gan Yan, Joshua T Vogelstein, F Xavier Castellanos, Adriana Di Martino, Clare Kelly, Keith Heberlein, Stan Colcombe, and Michael P Milham. Imaging human connectomes at the macroscale. *Nature Methods*, 10(6):524–539, June 2013. ISSN 1548-7091, 1548-7105. doi: 10.1038/nmeth.2482.
 - [20] Olaf Sporns, Giulio Tononi, and Rolf Kötter. The Human Connectome: A Structural Description of the Human Brain. *PLoS Computational Biology*, 1(4):e42, 2005. ISSN 1553-734X, 1553-7358. doi: 10.1371/journal.pcbi.0010042.
 - [21] Joshua T Vogelstein, Eric W Bridgeford, Benjamin D Pedigo, Jaewon Chung, Keith Levin, Brett Mensh, and Carey E Priebe. Connectal coding: Discovering the structures linking cognitive phenotypes to individual histories. *Current Opinion in Neurobiology*, 55:199–212, April 2019. ISSN 09594388. doi: 10.1016/j.conb.2019.04.005.
 - [22] Marcus Kaiser. A tutorial in connectome analysis: Topological and spatial features of brain networks. *NeuroImage*, 57(3):892–907, August 2011. ISSN 10538119. doi: 10.1016/j.neuroimage.2011.05.025.
 - [23] Mikail Rubinov and Olaf Sporns. Complex network measures of brain connectivity: Uses and

- interpretations. *NeuroImage*, 52(3):1059–1069, September 2010. ISSN 10538119. doi: 10.1016/j.neuroimage.2009.10.003.
- [24] Richard F. Betzel, John D. Medaglia, and Danielle S. Bassett. Diversity of meso-scale architecture in human and non-human connectomes. *Nature Communications*, 9(1):346, December 2018. ISSN 2041-1723. doi: 10.1038/s41467-017-02681-z.
 - [25] Jesús Arroyo and Elizaveta Levina. Simultaneous prediction and community detection for networks with application to neuroimaging. *arXiv:2002.01645 [stat]*, February 2020.
 - [26] Lu Wang, Zhengwu Zhang, and David Dunson. Symmetric Bilinear Regression for Signal Subgraph Estimation. *IEEE Transactions on Signal Processing*, 67(7):1929–1940, April 2019. ISSN 1053-587X, 1941-0476. doi: 10.1109/TSP.2019.2899818.
 - [27] Shangsi Wang, Cencheng Shen, Alexandra Badea, Carey E. Priebe, and Joshua T. Vogelstein. Signal Subgraph Estimation Via Vertex Screening. *arXiv:1801.07683 [stat]*, January 2018.
 - [28] J. T. Vogelstein, W. G. Roncal, R. J. Vogelstein, and C. E. Priebe. Graph Classification Using Signal-Subgraphs: Applications in Statistical Connectomics. *IEEE Transactions on Pattern Analysis and Machine Intelligence*, 35(7):1539–1551, July 2013. ISSN 0162-8828, 2160-9292. doi: 10.1109/TPAMI.2012.235.
 - [29] Martijn P. van den Heuvel, Edward T. Bullmore, and Olaf Sporns. Comparative Connectomics. *Trends in Cognitive Sciences*, 20(5):345–361, May 2016. ISSN 13646613. doi: 10.1016/j.tics.2016.03.001.
 - [30] Hang Chen, Vahan Huroyan, Utkarsh Soni, Yafeng Lu, Ross Maciejewski, and Stephen Kobourov. Same Stats, Different Graphs: Exploring the Space of Graphs in Terms of Graph Properties. *IEEE Transactions on Visualization and Computer Graphics*, pages 1–1, 2019. ISSN 1077-2626, 1941-0506, 2160-9306. doi: 10.1109/TVCG.2019.2946558.
 - [31] Jaewon Chung, Eric Bridgeford, Jesús Arroyo, Benjamin D. Pedigo, Ali Saad-Eldin, Vivek Gopalakrishnan, Liang Xiang, Carey E. Priebe, and Joshua T. Vogelstein. Statistical connectomics. *Annual Review of Statistics and Its Application*, 8(1):463–492, 2021. doi: 10.1146/annurev-statistics-042720-023234. URL <https://doi.org/10.1146/annurev-statistics-042720-023234>.
 - [32] Nian Wang, Robert J Anderson, David G Ashbrook, Vivek Gopalakrishnan, Youngser Park, Carey E Priebe, Yi Qi, Rick Laoprasert, Joshua T Vogelstein, Robert W Williams, and G Allan Johnson. Variability and Heritability of Mouse Brain Structure: Microscopic MRI Atlases and Connectomes for Diverse Strains. *NeuroImage*, page 117274, August 2020. ISSN 10538119. doi: 10.1016/j.neuroimage.2020.117274.
 - [33] Jill L Silverman, Seda S Tolu, Charlotte L Barkan, and Jacqueline N Crawley. Repetitive Self-Grooming Behavior in the BTBR Mouse Model of Autism is Blocked by the mGluR5 Antagonist MPEP. *Neuropsychopharmacology*, 35(4):976–989, March 2010. ISSN 0893-133X, 1740-634X. doi: 10.1038/npp.2009.201.
 - [34] H. G. McFarlane, G. K. Kusek, M. Yang, J. L. Phoenix, V. J. Bolivar, and J. N. Crawley. Autism-like behavioral phenotypes in BTBR T+tf/J mice. *Genes, Brain and Behavior*, 7(2):152–163, March 2008. ISSN 1601-1848, 1601-183X. doi: 10.1111/j.1601-183X.2007.00330.x.
 - [35] Maria Luisa Scattoni, Shruti U. Gandhi, Laura Ricceri, and Jacqueline N. Crawley. Unusual Repertoire of Vocalizations in the BTBR T+tf/J Mouse Model of Autism. *PLoS ONE*, 3(8):e3067, August 2008. ISSN 1932-6203. doi: 10.1371/journal.pone.0003067.
 - [36] Jacob Ellegood, Brooke A. Babineau, R. Mark Henkelman, Jason P. Lerch, and Jacqueline N. Crawley. Neuroanatomical analysis of the BTBR mouse model of autism using magnetic resonance imaging and diffusion tensor imaging. *NeuroImage*, 70:288–300, April 2013. ISSN 10538119. doi: 10.1016/j.neuroimage.2012.12.029.
 - [37] K.Z. Meyza and D.C. Blanchard. The BTBR mouse model of idiopathic autism – Current view on mechanisms. *Neuroscience & Biobehavioral Reviews*, 76:99–110, May 2017. ISSN 01497634. doi: 10.1016/j.neubiorev.2016.12.037.

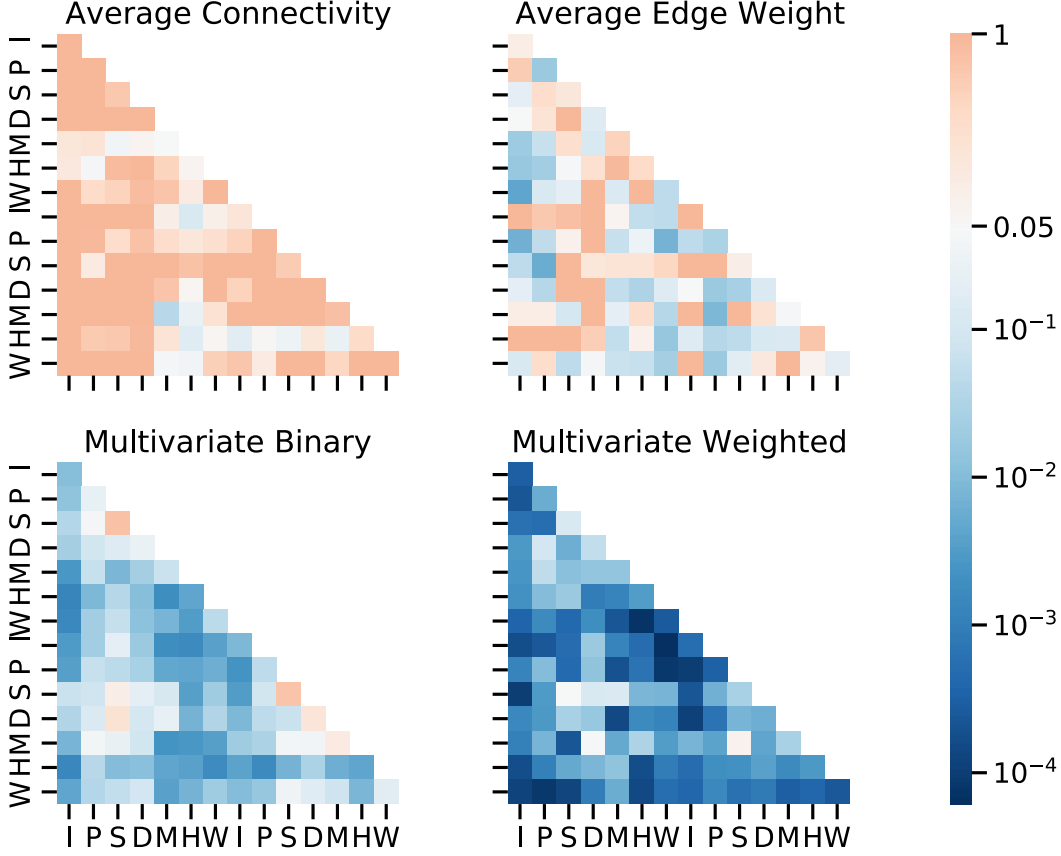
- [38] G. Allan Johnson, Alexandra Badea, Jeffrey Brandenburg, Gary Cofer, Boma Fubara, Song Liu, and Jonathan Nissanov. Waxholm Space: An image-based reference for coordinating mouse brain research. *NeuroImage*, 53(2):365–372, November 2010. ISSN 10538119. doi: 10.1016/j.neuroimage.2010.06.067.
- [39] Evan Calabrese, Alexandra Badea, Gary Cofer, Yi Qi, and G. Allan Johnson. A Diffusion MRI Tractography Connectome of the Mouse Brain and Comparison with Neuronal Tracer Data. *Cerebral Cortex*, 25(11):4628–4637, November 2015. ISSN 1047-3211, 1460-2199. doi: 10.1093/cercor/bhv121.
- [40] Dale Dagenbach. Insights into cognition from network science analyses of human brain functional connectivity: Working memory as a test case. In *Connectomics*, pages 27–41. Elsevier, 2019. ISBN 978-0-12-813838-0. doi: 10.1016/B978-0-12-813838-0.00002-9.
- [41] Gaël Varoquaux and R. Cameron Craddock. Learning and comparing functional connectomes across subjects. *NeuroImage*, 80:405–415, October 2013. ISSN 10538119. doi: 10.1016/j.neuroimage.2013.04.007.
- [42] Gábor J. Székely, Maria L. Rizzo, and Nail K. Bakirov. Measuring and testing dependence by correlation of distances. *The Annals of Statistics*, 35(6):2769–2794, December 2007. ISSN 0090-5364. doi: 10.1214/009053607000000505.
- [43] Sambit Panda, Satish Palaniappan, Junhao Xiong, Eric W. Bridgeford, Ronak Mehta, Cencheng Shen, and Joshua T. Vogelstein. Hyppo: A Comprehensive Multivariate Hypothesis Testing Python Package. *arXiv:1907.02088 [cs, stat]*, August 2020.
- [44] Andrew Zalesky, Alex Fornito, and Edward T. Bullmore. Network-based statistic: Identifying differences in brain networks. *NeuroImage*, 53(4):1197–1207, December 2010. ISSN 10538119. doi: 10.1016/j.neuroimage.2010.06.041.
- [45] Hugo C. Baggio, Alexandra Abos, Barbara Segura, Anna Campabadal, Anna Garcia-Diaz, Carme Uribe, Yaroslau Compta, Maria Jose Marti, Francesc Valldeoriola, and Carme Junque. Statistical inference in brain graphs using threshold-free network-based statistics. *Human Brain Mapping*, 39(6):2289–2302, June 2018. ISSN 1065-9471, 1097-0193. doi: 10.1002/hbm.24007.
- [46] Kwangsun Yoo, Peter Lee, Moo K. Chung, William S. Sohn, Sun Ju Chung, Duk L. Na, Daheon Ju, and Yong Jeong. Degree-based statistic and center persistency for brain connectivity analysis. *Human Brain Mapping*, 38(1):165–181, January 2017. ISSN 1065-9471, 1097-0193. doi: 10.1002/hbm.23352.
- [47] R Cameron Craddock, Rosalia L Tungaraza, and Michael P Milham. Connectomics and new approaches for analyzing human brain functional connectivity. *GigaScience*, 4(1):13, December 2015. ISSN 2047-217X. doi: 10.1186/s13742-015-0045-x.
- [48] Alex Fornito, Andrew Zalesky, and Michael Breakspear. Graph analysis of the human connectome: Promise, progress, and pitfalls. *NeuroImage*, 80:426–444, October 2013. ISSN 10538119. doi: 10.1016/j.neuroimage.2013.04.087.
- [49] Jinhui Wang, Xindi Wang, Mingrui Xia, Xuhong Liao, Alan Evans, and Yong He. GRETNA: A graph theoretical network analysis toolbox for imaging connectomics. *Frontiers in Human Neuroscience*, 9, June 2015. ISSN 1662-5161. doi: 10.3389/fnhum.2015.00386.
- [50] Avanti Athreya, Donniell E. Fishkind, Keith Levin, Vince Lyzinski, Youngser Park, Yichen Qin, Daniel L. Sussman, Minh Tang, Joshua T. Vogelstein, and Carey E. Priebe. Statistical inference on random dot product graphs: A survey. *arXiv:1709.05454 [math, stat]*, September 2017.
- [51] Keith Levin, Avanti Athreya, Minh Tang, Vince Lyzinski, and Carey E. Priebe. A Central Limit Theorem for an Omnibus Embedding of Multiple Random Dot Product Graphs. In *2017 IEEE International Conference on Data Mining Workshops (ICDMW)*, pages 964–967, New Orleans, LA, November 2017. IEEE. ISBN 978-1-5386-3800-2. doi: 10.1109/ICDMW.2017.132.
- [52] Sean L. Simpson, Satoru Hayasaka, and Paul J. Laurienti. Exponential Random Graph Modeling for Complex Brain Networks. *PLoS ONE*, 6(5):e20039, May 2011. ISSN 1932-6203. doi: 10.1371/journal.pone.0020039.

- [53] Junghi Kim, Jeffrey R. Wozniak, Bryon A. Mueller, Xiaotong Shen, and Wei Pan. Comparison of statistical tests for group differences in brain functional networks. *NeuroImage*, 101:681–694, November 2014. ISSN 10538119. doi: 10.1016/j.neuroimage.2014.07.031.
- [54] John W. Emerson, Walton A. Green, Barret Schloerke, Jason Crowley, Dianne Cook, Heike Hofmann, and Hadley Wickham. The Generalized Pairs Plot. *Journal of Computational and Graphical Statistics*, 22(1):79–91, January 2013. ISSN 1061-8600, 1537-2715. doi: 10.1080/10618600.2012.694762.
- [55] Nobuyuki Otsu. A Threshold Selection Method from Gray-Level Histograms. *IEEE Transactions on Systems, Man, and Cybernetics*, 9(1):62–66, January 1979. ISSN 0018-9472, 2168-2909. doi: 10.1109/TSMC.1979.4310076.
- [56] Michael A. A. Cox and Trevor F. Cox. *Multidimensional Scaling*, pages 315–347. Springer Berlin Heidelberg, Berlin, Heidelberg, 2008. ISBN 978-3-540-33036-3 978-3-540-33037-0. doi: 10.1007/978-3-540-33037-0_14.
- [57] Richard E. Passingham, Klaas E. Stephan, and Rolf Kötter. The anatomical basis of functional localization in the cortex. *Nature Reviews Neuroscience*, 3(8):606–616, August 2002. ISSN 1471-003X, 1471-0048. doi: 10.1038/nrn893.
- [58] Rogier B. Mars, Richard E. Passingham, and Saad Jbabdi. Connectivity Fingerprints: From Areal Descriptions to Abstract Spaces. *Trends in Cognitive Sciences*, 22(11):1026–1037, November 2018. ISSN 13646613. doi: 10.1016/j.tics.2018.08.009.
- [59] Xueqin Wang, Canhong Wen, Wenliang Pan, and Mian Huang. Sure Independence Screening Adjusted for Confounding Covariates with Ultrahigh-dimensional Data. *Statistica Sinica*, 2017. ISSN 10170405. doi: 10.5705/ss.202014.0117.
- [60] Guido W. Imbens and Donald B. Rubin. *Causal Inference for Statistics, Social, and Biomedical Sciences: An Introduction*. Cambridge University Press, first edition, April 2015. ISBN 978-0-521-88588-1 978-1-139-02575-1. doi: 10.1017/CBO9781139025751.
- [61] F. J. Anscombe. Graphs in statistical analysis. 27(1):17–21, 1973. ISSN 0003-1305, 1537-2731. doi: 10.1080/00031305.1973.10478966. URL <http://www.tandfonline.com/doi/abs/10.1080/00031305.1973.10478966>.
- [62] Karl-Heinz Nenning, Ting Xu, Ernst Schwartz, Jesus Arroyo, Adelheid Woehrer, Alexandre R. Franco, Joshua T. Vogelstein, Daniel S. Margulies, Hesheng Liu, Jonathan Smallwood, Michael P. Milham, and Georg Langs. Joint embedding: A scalable alignment to compare individuals in a connectivity space. *NeuroImage*, 222:117232, November 2020. ISSN 10538119. doi: 10.1016/j.neuroimage.2020.117232.
- [63] Ting Xu, Karl-Heinz Nenning, Ernst Schwartz, Seok-Jun Hong, Joshua T. Vogelstein, Alexandros Goulas, Damien A. Fair, Charles E. Schroeder, Daniel S. Margulies, Jonny Smallwood, Michael P. Milham, and Georg Langs. Cross-species functional alignment reveals evolutionary hierarchy within the connectome. *NeuroImage*, 223:117346, December 2020. ISSN 10538119. doi: 10.1016/j.neuroimage.2020.117346.
- [64] Joshua T. Vogelstein, William Gray Roncal, R. Jacob Vogelstein, and Carey E. Priebe. Graph classification using signal-subgraphs: Applications in statistical connectomics. *IEEE Transactions on Pattern Analysis and Machine Intelligence*, 35(7):1539–1551, 2013. doi: 10.1109/TPAMI.2012.235.
- [65] Jaewon Chung, Benjamin D. Pedigo, Eric W. Bridgeford, Bijan K. Varjavand, Hayden S. Helm, and Joshua T. Vogelstein. GraSPy: Graph statistics in python. *Journal of Machine Learning Research*, 20(158):1–7, 2019.
- [66] In Jae Myung. The importance of complexity in model selection. *Journal of Mathematical Psychology*, 44(1):190–204, 2000. ISSN 0022-2496. doi: <https://doi.org/10.1006/jmps.1999.1283>. URL <https://www.sciencedirect.com/science/article/pii/S002224969991283X>.
- [67] Soham Dan and Bhaswar B. Bhattacharya. Goodness-of-fit tests for inhomogeneous random graphs. In Hal Daumé III and Aarti Singh, editors, *Proceedings of the 37th International Confer-*

- ence on Machine Learning, volume 119 of *Proceedings of Machine Learning Research*, pages 2335–2344. PMLR, 13–18 Jul 2020. URL <http://proceedings.mlr.press/v119/dan20a.html>.
- [68] Cencheng Shen and Joshua T. Vogelstein. The Chi-Square Test of Distance Correlation. *arXiv:1912.12150 [cs, math, stat]*, February 2020.
 - [69] Joshua L Morgan and Jeff W Lichtman. Why not connectomics? *Nature Methods*, 10(6):494–500, June 2013. ISSN 1548-7091, 1548-7105. doi: 10.1038/nmeth.2480.
 - [70] Patrick E. Myers, Ganesh C. Arvapalli, Sandhya C. Ramachandran, Derek A. Pisner, Paige F. Frank, Allison D. Lemmer, Eric W. Bridgeford, Aki Nikolaidis, and Joshua T. Vogelstein. Standardizing Human Brain Parcellations. Preprint, Neuroscience, November 2019.
 - [71] Christopher R. Genovese, Nicole A. Lazar, and Thomas Nichols. Thresholding of Statistical Maps in Functional Neuroimaging Using the False Discovery Rate. *NeuroImage*, 15(4):870–878, April 2002. ISSN 10538119. doi: 10.1006/nimg.2001.1037.
 - [72] Bradley Efron. Simultaneous inference: When should hypothesis testing problems be combined? *The Annals of Applied Statistics*, 2(1):197–223, March 2008. ISSN 1932-6157. doi: 10.1214/07-AOAS141.
 - [73] Sture Holm. A Simple Sequentially Rejective Multiple Test Procedure. *Scandinavian Journal of Statistics*, 6(2):65–70, 1979. ISSN 0303-6898.
 - [74] Eric W. Weisstein. Bonferroni Correction. {From MathWorld—A Wolfram Web Resource}, 2004.
 - [75] Gregory Kiar, Eric W. Bridgeford, William R. Gray Roncal, Consortium for Reliability and Reproducibility (CoRR), Vikram Chandrashekar, Disa Mhembere, Sephira Ryman, Xi-Nian Zuo, Daniel S. Margulies, R. Cameron Craddock, Carey E. Priebe, Rex Jung, Vince D. Calhoun, Brian Caffo, Randal Burns, Michael P. Milham, and Joshua T. Vogelstein. A High-Throughput Pipeline Identifies Robust Connectomes But Troublesome Variability. Preprint, Neuroscience, September 2017.
 - [76] Peter D Hoff, Adrian E Raftery, and Mark S Handcock. Latent Space Approaches to Social Network Analysis. *Journal of the American Statistical Association*, 97(460):1090–1098, December 2002. ISSN 0162-1459, 1537-274X. doi: 10.1198/016214502388618906.
 - [77] Edward R. Scheinerman and Kimberly Tucker. Modeling graphs using dot product representations. *Computational Statistics*, 25(1):1–16, March 2010. ISSN 0943-4062, 1613-9658. doi: 10.1007/s00180-009-0158-8.
 - [78] Paul W. Holland, Kathryn Blackmond Laskey, and Samuel Leinhardt. Stochastic blockmodels: First steps. *Social Networks*, 5(2):109–137, June 1983. ISSN 03788733. doi: 10.1016/0378-8733(83)90021-7.
 - [79] Fang-Cheng Yeh, Timothy D. Verstynen, Yibao Wang, Juan C. Fernández-Miranda, and Wen-Yih Isaac Tseng. Deterministic diffusion fiber tracking improved by quantitative anisotropy. 8(11): e80713. ISSN 1932-6203. doi: 10.1371/journal.pone.0080713. URL <https://dx.plos.org/10.1371/journal.pone.0080713>.
 - [80] Fang-Cheng Yeh and Wen-Yih Isaac Tseng. NTU-90: A high angular resolution brain atlas constructed by q-space diffeomorphic reconstruction. *NeuroImage*, 58(1):91–99, September 2011. ISSN 10538119. doi: 10.1016/j.neuroimage.2011.06.021.
 - [81] Fang-Cheng Yeh, Van Jay Wedeen, and Wen-Yih Isaac Tseng. Generalized $\{Q\}$ -Sampling Imaging. *IEEE Transactions on Medical Imaging*, 29(9):1626–1635, September 2010. ISSN 0278-0062, 1558-254X. doi: 10.1109/TMI.2010.2045126.
 - [82] Fang-Cheng Yeh, Li Liu, T. Kevin Hitchens, and Yijun L. Wu. Mapping immune cell infiltration using restricted diffusion MRI: Restricted Diffusion Imaging. *Magnetic Resonance in Medicine*, 77(2): 603–612, February 2017. ISSN 07403194. doi: 10.1002/mrm.26143.
 - [83] Zuguang Gu, Roland Eils, and Matthias Schlesner. Complex heatmaps reveal patterns and correlations in multidimensional genomic data. *Bioinformatics*, 32(18):2847–2849, September 2016. ISSN 1367-4803, 1460-2059. doi: 10.1093/bioinformatics/btw313.

Appendix A. Supplementary investigations of real data.

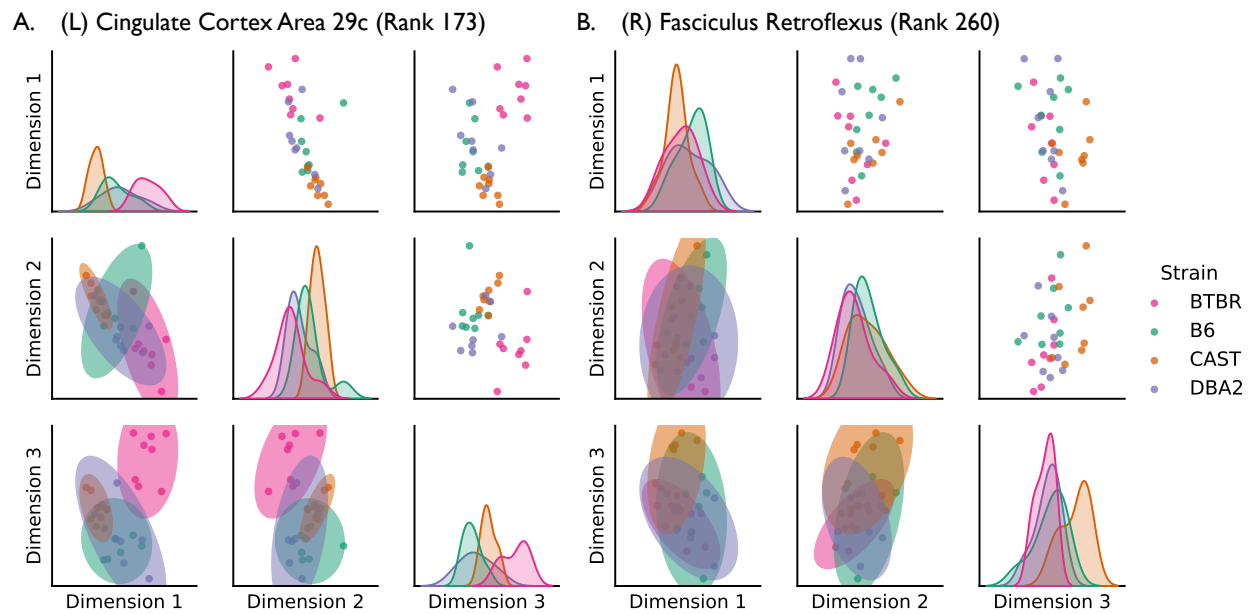
Comparison of mesoscale methods In Supplementary Figure 4, we show the log-transformed p -value for each approach, with communities in blue denoting signal communities (significant after Holm–Bonferroni correction).



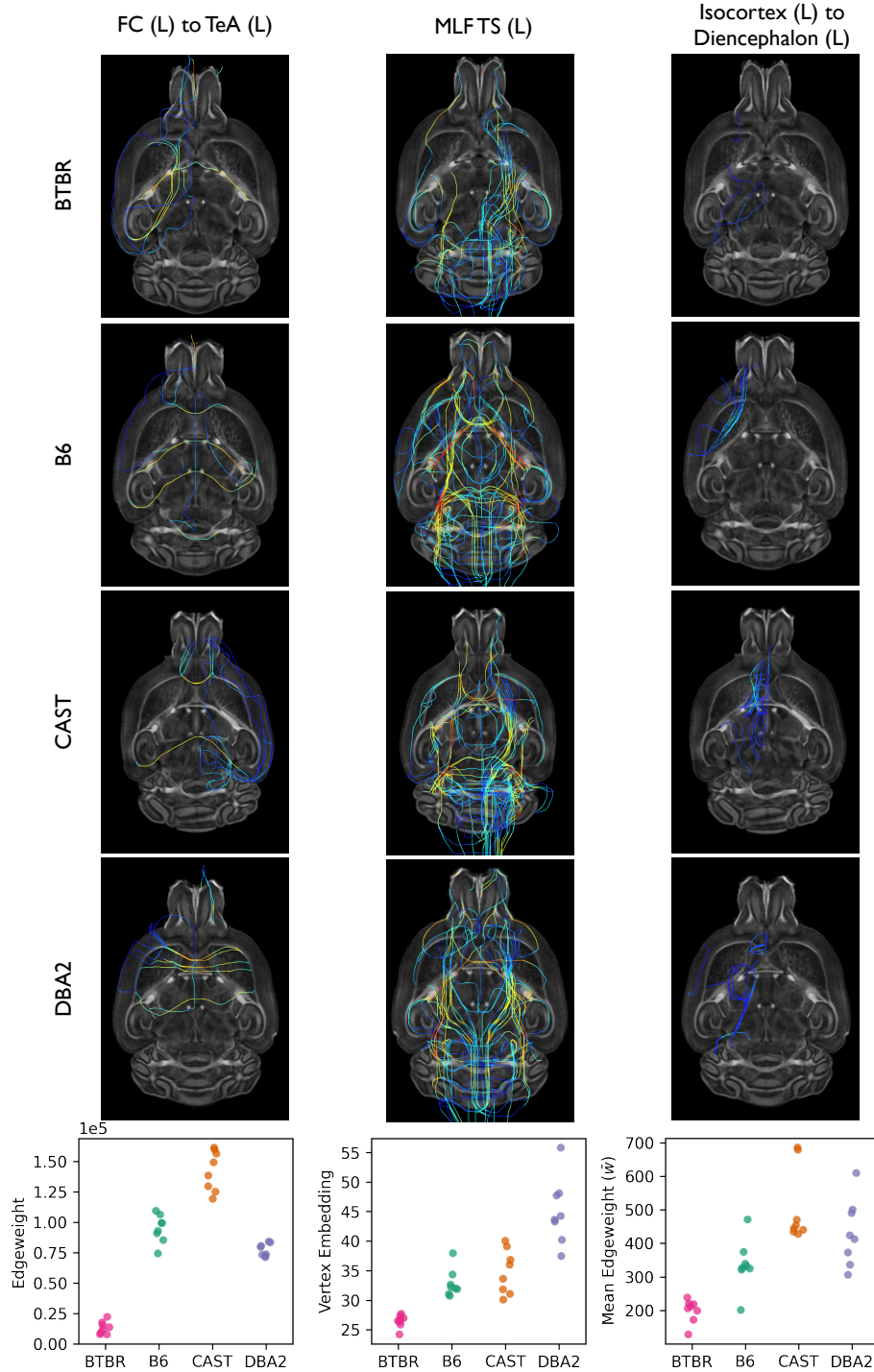
Supplementary Figure 4: P -values for each proposed approach for summarizing the information in a community. More signal communities are found as the amount of information encoded by the summary method increases. Because connectomes in this dataset are undirected, this significance matrix will be symmetric and therefore only the upper triangle of these matrices should be considered. The colorbar represents $\log_{10} p$ -values. Significance is determined at $\alpha = 0.05$ following Holm–Bonferroni correction; therefore, communities in blue are signal communities.

Embeddings of weak signal vertices The strongest signal vertex identified by this method in our real-world data was the left hemisphere corpus callosum. In Figure 3, we demonstrate how a *pairs plot*, a d -dimensional scatter plot matrix, can be used to visualize the vertex embedding produced by OMNI. In Supplementary Figure 5, we show pairs plots of two weak signal vertices for comparison.

Visualizing null edges, vertices, and communities Using the procedures described above, we identified the weakest signal edge (the left frontal cortex to the right temporal association cortex), vertex (the left medial longitudinal fasciculus and tectospinal tract), and community (left isocortex to left diencephalon) across all mouse strains. To contrast with the strongest signal structures shown in Figure 4, we plotted tractograms of the weakest components neurological structures (Supplementary Figure 6). These tractograms are much more homogeneous than those plotted in Figure 4, as are the distributions of numerical features for each component (shown in the bottom row). Since this edge, vertex, and community contain no information about the strain of a mouse, we term them *null components*.



Supplementary Figure 5: Pairs plots of the vertex embeddings of the left cingulate cortex area 29c and the right fasciculus retroflexus, two weak signal vertices identified by DMMI and MANOVA . As shown by the kernel density estimates (*diagonal*) and the 95% prediction ellipses (*lower triangle*), the distribution of these embeddings is not separable. This emphasizes the homogeneity of these vertices across strains relative to the two strongest signal vertices shown in Figure 3.



Supplementary Figure 6: Visualization of the weakest signal edge (the left frontal cortex to the right temporal association cortex), vertex (the left medial longitudinal fasciculus and tectospinal tract), and community (left isocortex to left diencephalon) across all mouse strains. At each topological scale, tractograms of these neurological structures are shown for each mouse strain. Compared to Figure 4, tractograms here are much more homogeneous across strains, displaying minor differences in connectivity. (*Bottom row*) The distribution of edge weights for the weakest signal edge (*Column 1*); the distribution of the first embedding dimension for the weakest signal vertex (*Column 2*); and the distribution of average edge weight for the most weakest signal community (*Column 3*). Each dot represents data from an individual mouse. Differences in distributions are much less pronounced compared to Figure 4. In these distributions, one strain is typically aberrant while the other three strains are homogeneous.

Appendix B. Statistical rankings of signal components.

Vertex 1	Vertex 2	statistic	p-value
Corpus Callosum (L)	Striatum (R)	0.717	0.053
Corpus Callosum (L)	Internal Capsule (R)	0.699	0.070
Corpus Callosum (L)	Reticular Nucleus of Thalamus (R)	0.698	0.072
Corpus Callosum (L)	Zona Incerta (R)	0.686	0.088
Septum (R)	Corpus Callosum (R)	0.671	0.113
Striatum (L)	Striatum (R)	0.664	0.127
Corpus Callosum (L)	Ventral Thalamic Nuclei (R)	0.663	0.128
Hippocampus (L)	Middle Cerebellar Peduncle (L)	0.658	0.139
Caudomedial Entorhinal Cortex (R)	Ventral Hippocampal Commissure (R)	0.656	0.145
Corpus Callosum (L)	Midbrain Reticular Nucleus (R)	0.653	0.154
Midbrain Reticular Nucleus (L)	Superior Cerebellar Peduncle (L)	0.648	0.166
Corpus Callosum (L)	Corpus Callosum (R)	0.646	0.172
Spinal Trigeminal Nerve (L)	Middle Cerebellar Peduncle (L)	0.645	0.173
Secondary Visual Cortex L (L)	Striatum (R)	0.641	0.185
Globus Pallidus (R)	Midbrain Reticular Nucleus (R)	0.632	0.217
Striatum (L)	Corpus Callosum (R)	0.632	0.217
Primary Somatosensory Cortex HL (L)	Secondary Visual Cortex MM (L)	0.629	0.228
Corpus Callosum (L)	Primary Somatosensory Cortex J (R)	0.628	0.230
Corpus Callosum (L)	Ventral Orbital Cortex (R)	0.628	0.231
Zona Incerta (R)	Intermediate Reticular Nucleus (R)	0.627	0.234

Table 1: The top 20 signal edges (out of 54,946 total edges) ranked by the order of their Holm–Bonferroni corrected p -value. Eleven of the top 20 signal edges are adjacent to either the left or right hemisphere corpus callosum.

Vertex	Pillai	F(15, 78)	p-value
Corpus Callosum (L)	2.592	33.026	4.47e-25
Corpus Callosum (R)	2.550	29.501	1.75e-23
Secondary Motor Cortex (L)	2.438	22.578	7.73e-20
Midbrain Reticular Nucleus (R)	2.435	22.429	9.43e-20
Fimbria (L)	2.424	21.902	1.94e-19
Substantia Nigra (R)	2.299	17.049	3.04e-16
Secondary Motor Cortex (R)	2.298	17.034	3.10e-16
Internal Capsule (R)	2.297	17.003	3.26e-16
Striatum (L)	2.259	15.854	2.32e-15
Cerebral Peduncle (R)	2.229	15.036	9.98e-15
Internal Capsule (L)	2.219	14.775	1.60e-14
Stria Terminalis (R)	2.209	14.514	2.59e-14
Cerebellar White Matter (R)	2.204	14.409	3.14e-14
Optic Tracts (L)	2.194	14.166	4.95e-14
Hippocampus (R)	2.185	13.952	7.43e-14
Subthalamic Nucleus (L)	2.176	13.738	1.12e-13
Frontal Association Cortex (L)	2.175	13.702	1.19e-13
Stria Terminalis (L)	2.174	13.679	1.25e-13
Retro Rubral Field (R)	2.167	13.537	1.64e-13
Rostral Linear Nucleus (R)	2.159	13.350	2.35e-13

Table 2: The top 20 signal vertices (out of 326 total vertices) ranked by the order of their Holm–Bonferroni corrected p -values. Pillai’s trace and approximate F statistic (along with degrees of freedom) as calculated by one-way MANOVA are also reported. The corpus callosum in the left and right hemisphere are the top two signal vertices.

Vertex	statistic	p-value
Substantia Nigra (L)	0.855	3.28e-05
Middle Cerebellar Peduncle (R)	0.852	3.45e-05
Internal Capsule (L)	0.851	3.5e-05
Substantia Nigra (R)	0.845	3.84e-05
Pontine Reticular Nucleus (R)	0.840	4.14e-05
Pontine Reticular Nucleus (L)	0.838	4.25e-05
Parasubiculum (L)	0.838	4.25e-05
Ventral Tegmental Area (R)	0.837	4.32e-05
Retro Rubral Field (L)	0.829	4.91e-05
Fastigial Medial Nucleus of Cerebellum (R)	0.824	5.3e-05
Cerebral Peduncle (R)	0.819	5.74e-05
Cerebral Peduncle (L)	0.818	5.87e-05
Fastigial Medial Nucleus of Cerebellum (L)	0.814	6.23e-05
Fimbria (L)	0.813	6.28e-05
Brain Stem Rest (L)	0.811	6.46e-05
Cingulate Cortex Area 30 (L)	0.810	6.6e-05
Ventral Tegmental Area (L)	0.806	6.99e-05
Globus Pallidus (R)	0.802	7.46e-05
Internal Capsule (R)	0.797	8.09e-05
Subthalamic Nucleus (R)	0.792	8.78e-05
Zona Incerta (R)	0.783	0.000102
Parabrachial Nucleus (L)	0.783	0.000102
Globus Pallidus (L)	0.781	0.000104
Insular Cortex (R)	0.780	0.000106
Brain Stem Rest (R)	0.777	0.00011
Secondary Visual Cortex Mediolateral Area (R)	0.777	0.00011
Inferior Colliculus (R)	0.776	0.000111
Superior Cerebellar Peduncle (L)	0.775	0.000113
Retro Rubral Field (R)	0.773	0.000117
Stria Terminalis (L)	0.772	0.000118
Postsubiculum (R)	0.769	0.000123
Midbrain Reticular Nucleus (L)	0.768	0.000125
Striatum (R)	0.768	0.000125
Primary Visual Cortex Binocular Area (R)	0.768	0.000125
Corpus Callosum (L)	0.767	0.000125

Table 3: The top 34 vertices (out of 326 total vertices) as detected by MDMR, ranked by the order of their Holm–Bonferroni corrected p -values. MDMR is a weak statistical test for detecting signal vertices given that the corpus callosum is the 34th ranked vertex.

	<i>Left Hemisphere</i>		<i>Right Hemisphere</i>		
Vertex	p-value	Rank	p-value	Rank	Avg. Rank
Corpus Callosum	4.47e-25	1	1.75e-23	2	1.5
Secondary Motor Cortex	7.73e-20	3	3.1e-16	7	5.0
Internal Capsule	1.6e-14	11	3.26e-16	8	9.5
Stria Terminalis	1.25e-13	18	2.59e-14	12	15.0
Fimbria	1.94e-19	5	3.58e-12	26	15.5
Ventral Tegmental Area	3.87e-12	27	8.76e-13	21	24.0
Hippocampus	8.02e-11	40	7.43e-14	15	27.5
Ectorhinal Cortex	8.11e-12	29	4.56e-11	37	33.0
Globus Pallidus	9.68e-11	41	1.89e-12	25	33.0
Cerebral Peduncle	4.64e-10	57	9.98e-15	10	33.5

Table 4: The top 10 bilateral signal vertex pairs (out of 163 total vertex pairs) ranked by the order of their average rank.

Community 1	Community 2	statistic	p-value
White Matter (R)	White Matter (R)	0.885	6.43e-06
White Matter (L)	White Matter (L)	0.857	1.02e-05
Hindbrain (L)	White Matter (L)	0.849	1.14e-05
Midbrain (R)	White Matter (R)	0.845	1.21e-05
Isocortex (L)	Isocortex (L)	0.844	1.22e-05
Pallium (R)	White Matter (R)	0.831	1.5e-05
Isocortex (R)	White Matter (R)	0.823	1.68e-05
Isocortex (R)	Isocortex (R)	0.819	1.8e-05
Isocortex (L)	White Matter (L)	0.811	2.02e-05
Hindbrain (R)	White Matter (R)	0.810	2.02e-05

Table 5: The top 10 signal communities (out of 105 total communities) ranked by the order of their Holm–Bonferroni corrected p -values as calculated by the Multivariate Weighted method.